Archaeological and Anthropological Sciences (2026) 18:24
https://doi.org/10.1007/s12520-025-02380-7

RESEARCH

'Cervified': a new method for the morphometric identification of red deer (*Cervus elaphus*), fallow deer (*Dama dama*), and roe deer (*Capreolus capreolus*) postcranial bones from European archaeological contexts

Veronica Aniceti[1] · **Mauro Rizzetto**[2] · **Francesco Giacalone**[3]

Received: 10 May 2025 / Accepted: 27 November 2025 / Published online: 16 January 2026

Abstract
This paper presents a new method for differentiating postcranial bone remains of red deer (*Cervus elaphus*), fallow deer (*Dama dama*), and roe deer (*Capreolus capreolus*) from European archaeological contexts. These species have very similar bone morphology and partly overlapping size ranges, often preventing species-level identification in zooarchaeological research. Traditional methods, such as the use of diagnostic morphological criteria, or aDNA analysis, present practical and methodological limitations. In this study, bone biometric data from modern specimens, sourced from various institutions across northern and southern Europe, are analysed to determine size ranges and shape indices that can separate the three species, focussing on both adult and immature individuals. By comparing measurement values from archaeological remains against these biometric criteria, species identification can be attempted. The low-tech nature of this approach and the transparent, diagrammatic presentation of biometric results make the new method objective and highly accessible. In European and Mediterranean historical archaeology, the species-level identification of cervid remains is crucial in the investigation of biogeography, trading activities, hunting strategies, cultural values, and social status.

Keywords Red deer · Fallow deer · Roe deer · Method · Identification · Biometry · Archaeology

Introduction

Red deer, fallow deer, and roe deer are currently among the most widespread large- and medium-sized wild mammals in Europe and, not surprisingly, have often played an important role in human society. These animals were hunted as a source of food and other materials, whether as part of subsistence or recreational activities, held significant religious and magico-medicinal meaning, and could represent, alive or on the table, a symbol of social differentiation. As such, deer has been the subject of extensive literature (e.g., Chapman and Chapman 1975; Grant 1988; Soderberg 2004; Holmes 2014; Schmidt 2014; Miller and Sykes 2016; Albarella and Aniceti 2024; Almeida et al. 2024). In the last two decades, zooarchaeological research on this taxon has benefitted from methodological improvements and the application of new analytical techniques, from ageing tools (Bowen et al. 2016; Marín et al. 2024), to isotopic and genetic analyses (Skog et al. 2009; McDevitt and Zachos 2014; Sykes et al. 2016; Baker et el. 2024a; Baker et al. 2024b), to biometry (Carden et al. 2012; Sykes et al. 2013; Karastoyanova et al. 2020). This paper aims to contribute to a fundamental yet often overlooked aspect of cervid archaeological research, functional to many of the studies and techniques mentioned above, namely species-level identification of faunal remains.

Veronica Aniceti and Mauro Rizzetto contributed equally to this work.

✉ Veronica Aniceti
veronica.aniceti@imf.csic.es

✉ Mauro Rizzetto
mauro.rizzetto@vub.be

[1] Institución Milá y Fontanals de Investigación en Humanidades (IMF), CSIC, Barcelona, Spain

[2] Interdisciplinary Historical Food Studies Research Group (VUB-FOST), Vrije Universiteit Brussel, Brussels, Belgium

[3] ludwig.guru, Palermo, Italy

Fig. 1 Two female red deer (Norway). Photo credit: Bjørn Reidar Olsson

In zooarchaeology, the identification of the remains of red deer (*Cervus elaphus*), fallow deer (*Dama dama* – namely, the European fallow deer), and roe deer (*Capreolus capreolus*) has often posed significant challenges (Figs. 1, 2, and 3). The geographical distribution of these three species changed over time but often overlapped in Europe and other regions of the Mediterranean. Their bone morphological similarities and partial size overlaps, in addition to the fragmented nature of most faunal materials, often prevent species-level identification, limiting the interpretative potentials of the zooarchaeological evidence. The problem of identification of European cervid remains from historical times arises from the introduction and spread of the European fallow deer in the Continent since at least Roman times and then, more consistently, during the Middle Ages (Davis and MacKinnon 2009; Masseti and Vernesi 2014; Baker et al. 2024a, b). Indeed, this species partly overlaps in size with the red deer, which is larger, and, more rarely, with the roe deer, a smaller animal. The extent of such size overlaps in past animal populations is, however, often difficult to assess, due to substantial diachronic and spatial size variability. The

Fig. 2 A male fallow deer (United Kingdom). https://pixabay.com/ (royalty-free stock photos)

Fig. 3 A male roe deer (Norway). Photo credit: Bjørn Reidar Olsson

factors determining deer size ranges and their fluctuations are multiple. Sexual dimorphism is especially strong in red deer and fallow deer (Post et al. 1999; McElligott et al. 2001; Milošević-Zlatanović et al. 2016), implying size overlaps of large male fallow deer and small female red deer. Climatic conditions also impact on deer size, cervids being larger in colder periods or regions and therefore in the centre-north of the Continent (Toïgo et al. 2006; Apollonio and Chirichella 2023), as do specific geographical contexts such as islands and isolated regions, where these animals are smaller (Lister 1989; Mulville 2010). Predation as well can impact deer population structure and body size (Kjellander et al. 2004; Heurich et al. 2016). Finally, anthropogenic factors such as hunting pressure, habitat reduction, forced relocation, and emparkment have also shown to lead to a reduction in size (Serrano et al. 2007; Karastoyanova et al. 2020). In faunal assemblages, the potential presence of immature individuals, whether identifiable or not as such, leads to even greater size overlaps and can further compromise species-level identification. Currently, the separation of red, fallow, and roe deer archaeological remains is attempted through different and sometimes complementary methodologies:

- *Size analyses*. When large assemblages are available and through comparisons with data from related sites, it is sometimes possible to identify size clusters that can be attributed to different species (Davis and MacKinnon 2009; Aniceti et al. 2021; Albarella and Davis 1996). Large samples of cervid biometric values are, however, rarely available; in addition, size overlaps between species are frequent, for the reasons mentioned above, limiting the efficiency of species-level identification based on size alone.
- *Morphological criteria*. These have long been established for the distinction between red and fallow deer (Di Stefano 1995; Lister 1996), while general osteological atlases can offer additional support (e.g., Prat

1970; Pales and Garcia 1981). The use of morphological criteria, however, is inevitably biased by a certain degree of subjectivity and by the level of expertise of different researchers, and ideally requires the assistance of abundant reference material; in addition, not all criteria are equally diagnostic (Lister 1996), implying that taxonomic separation is more difficult and less reliable on some zones. More importantly, the results of such attempts cannot be objectively scrutinised by other researchers.

- *Ancient DNA* (*aDNA*). Genetic analyses can be very effective when enough collagen is preserved. aDNA analyses are not used with the specific purpose of separating fallow deer and red deer remains but rather to investigate genetic structures and past zoogeographical dynamics in these species; in doing so, however, some specimens considered in these studies are shown to belong to the other species and excluded (e.g., Baker et al. 2024a; Beglane et al. 2018). Despite their effectiveness, genetic analyses are nonetheless constrained by severe cost limitations and are destructive. Zooarchaeology by Mass Spectrometry (ZooMS), on the other hand, cannot currently separate between red and fallow deer remains (Buckley and Whitcher Kansa 2011). In addition, this technique too involves destructive procedures and can be economically impacting when applied to large samples, despite being less time-consuming and more affordable compared to genetic analyses.

This study introduces a new method for the separation of fallow deer from red deer and roe deer remains, that can be applied to European and central-western Mediterranean regions where these species co-existed – often as a result of human-mediated dispersals that began at least in the Roman period. The method consists in the use of biometric indices and size ranges, derived from modern cervid skeletons of known species, against which indices and raw measurement values from archaeological material can be plotted for comparison. Such approach implies a key set of advantages:

- It allows for more objective identification attempts, as these are represented graphically and therefore open to scrutiny;
- The separation potentials of size and shape are combined to maximize chances of reliable species-level identification;
- In some skeletal elements, diagnostic indices can also be used on immature individuals, when size alone is of no use, or on zones where no morphological criteria exist (e.g., long bone shafts);
- Lastly, the method relies on the use of the calliper and osteometric board and is therefore widely accessible.

The new method does not aim to replace the identification methods listed above, nor to dismiss any potential future improvements to such methods or the importance of an appropriate use of reference collections. Rather, it aims to provide additional support to the study of the history of cervids in Europe and the Mediterranean; in phylogenetic studies of fallow deer in a specific period or region, for example, the use of an efficient, objective, and inexpensive biometric method may assist in the identification of a more reliable sample of fallow deer bones on which to focus funds for genetic analyses. This biometric method relies on an extensive dataset which, on the other hand, is not exhaustive of all regions and available modern cervid skeletons; however, the variability in size ranges covered and the consistency in the distribution of shape index values ensure the applicability of the method to other regions, provided critical interpretation of the results is always used. Ultimately, more widespread and correct identification of cervid archaeological remains will contribute to the reconstruction of past biodiversity, human-animal-environment interactions, and socio-economic and cultural practices.

Materials and methods

Biometric data from modern red, fallow, and roe deer skeletal elements were collected between 2019 and 2024 from various institutions in northern and southern Europe (Table 1). The taxonomic and, when available, exact or estimated age-at-death, sex, and provenance information were recorded for each specimen.

The skeletal elements and zones to measure were selected based on the presence of measurable features, the likelihood of preservation in the archaeological record (i.e., denser and more robust elements/zones), and the probability of being recovered through hand-collection during excavation (i.e., larger elements) (Table 2). This prompted the exclusion of elements or zones such as the femur, as the late stage at which its epiphyses fuse, as well as its structure, mean this bone often lacks well-preserved measurable features; the proximal ends of the humerus and tibia, as well as the distal end of the radius, for the same reasons (although greatest length measurements, involving both the proximal and distal ends, have been analysed); and phalanges, as, although often recovered whole, they are more easily missed during hand-collection (like other smaller elements), and their anatomical position (as part of forelimbs or hindlimbs) can affect measurement ratios but is often difficult to determine. In addition, the atlas, axis, scapho-cuboid, and pelvis were excluded in the course of the study as preliminary analyses showed no potential for species-level identification. Finally, teeth were not considered in this study due to limitations in

Table 1 List of visited institutions with numbers of modern complete and partial skeletons measured for each species. * Includes specimens from the UK only

Country	Institution	Red deer	Fallow deer	Roe deer
Austria	Natural History Museum, Wien	23	14	16
Greece	Malcolm H. Wiener Laboratory for Archaeological Science, ASCSA*	1	3	3
Hungary	Hungarian Natural History Museum, Budapest	11	24	4
Italy	Department of Physical Sciences, Earth and Environment, Siena	7	19	6
	Natural History Museum, Venice	3	2	5
Norway	Department of Natural History-University Museum, Bergen	24	-	6
UK	Department of Archaeology, Sheffield	12	10	14
	Historic England, Portsmouth	30	17	24
	Sheila Hamilton Dyer's reference collection, Southampton	4	5	10
Total		**115**	**94**	**88**

selecting multiple distinct measurements required for combined size and shape analysis, owing to their conformation and the variability introduced by wear – characteristics that may make them better suited to geometric morphometric approaches. In sum, this selective focus allowed for the concentration of time and resources on those commonly recovered elements or zones with the greatest potential for species identification based on the employed morphometric criteria: scapula (glenoid cavity and neck), humerus (distal end and shaft), radius (proximal end), metacarpal (distal end and shaft), tibia (distal end and shaft), astragalus, calcaneum, and metatarsal (distal end and shaft).

Measurements were taken on the bones of adult and immature individuals. In this study, individuals were considered immature when one or more epiphyses of the element being measured were unfused. Most of the analyses of specific zones focused on specimens for which all epiphyses were fused or fusing, or fully ossified; for selected zones, immature specimens were analysed in separate graphs. The measurements chosen to develop the biometric method include standard ones, as well as new ones created to translate morphological traits, some of which had been previously identified as diagnostic (Di Stefano 1995; Lister 1996) (Table 2; Online Resource 1). All measurements were taken using 15-cm Mitutoyo digital callipers with a precision to the tenth of a millimetre, with the exception of long bone greatest lengths for which an osteometric board was used, with a precision to the millimetre. Raw data for all selected elements are available in Mendeley Data (https://data.mendeley.com/datasets/vn43dpvbzr/1), allowing researchers to reproduce the graphs and plot their own archaeological values against modern ranges.

The inter- and intra-observer errors were estimated in order to assess the reliability of use of each measurement, some of which are new or adapted, as well as the repeatability of results. The recording protocol was shared with seven zooarchaeologists from the Sheffield Zooarchaeology Laboratory (UK) with different levels of expertise in biometric analyses; therefore, the total number of researchers involved, including the authors, was nine. Each researcher took the measurements listed in Table 2 on modern adult skeletons of red deer (ID: 1205), fallow deer (ID: 1207), and roe deer (ID: 1584) from the laboratory's reference collection. To evaluate the consistency in data recording among observers, the Intraclass Correlation Coefficient (ICC) was employed, a standard statistical method for assessing reproducibility and inter-observer agreement in quantitative studies (Koo and My 2016). For the assessment of intra-observer reliability, the authors measured the same three specimens repeatedly across three days at different times of the day. The inter- and intra-observer error results are reported and discussed in Online Resource 2. In general, very high ICC values were obtained, indicating an excellent inter-observer and intra-observer reliability for most measurements.

Absolute measurement values and relative values (i.e., shape indices) were grouped and analysed by species (three variables) and age (synthesized in two variables, adult and immature, as described above), without any further separation based on sex or geographical provenance. The exclusion of sexual and geographical variables reflects the fact that their influence on size and shape ranges can change substantially through time, as a consequence of climatic and environmental changes (Apollonio and Chirichella 2023), changes in local faunal composition (Heurich et al. 2016), animal mobility, or anthropogenic factors (Sykes et al. 2013). Therefore, while the nature of such variables, as discernible from the available dataset, is of significant interest for current cervid morphometry (Aniceti et al., in prep.), they should not be taken into account when constructing a method intended for application to archaeological materials: restricting value ranges based on the selection of regional data assumes that no morphometric changes occurred in deer species over centuries or millennia, creating the illusion of easier taxonomic identification, while separately marking values from female and male specimens would lead to a similar overinterpretation of the archaeological evidence. In sum, the present method captures as much variability as possible based on the available modern data,

Table 2 List of measurements taken on each element. Italic: measurements also used in analyses focussing specifically on immature elements. +: newly introduced measurements. For visual descriptions of the new measurements see Online Resource (OR) 1

Element	Measurement	Description	Reference(s)
scapula	SLC	Smallest length of the *collum scapulae* (neck)	von den Driesch 1976
	GLP	Greatest length of the *processus articularis*	von den Driesch 1976
	LG	Length of the glenoid cavity	von den Driesch 1976
	BG	Breadth of the glenoid cavity	von den Driesch 1976
	ASG	Shortest distance from the base of the spine to edge of glenoid cavity	Salvagno and Albarella 2017, adapted from Fernández 2001's DEB
humerus	GLC	Greatest length from the *caput* (head)	von den Driesch 1976
	SD	Smallest breadth of the diaphysis	von den Driesch 1976
+	*SD1*	Smallest depth of the diaphysis	OR1 Fig. 1
	BT	Greatest breadth of the trochlea	von den Driesch 1976
	Bd	Greatest breadth of the distal end	von den Driesch 1976
	HTC	Vertical/smallest diameter of the trochlea at its central constriction	Payne and Bull 1988
+	HX	Lateral height of the trochlea	OR1 Fig. 2
+	HTL	Vertical/smallest diameter of the capitulum at its constriction	OR1 Fig. 2
radius	GL	Greatest length	von den Driesch 1976
	SD	Smallest breadth of the diaphysis	von den Driesch 1976
+	*SD1*	Smallest depth of the diaphysis (only when the ulna is not attached to the radius)	OR1 Fig. 3
	Bp	Greatest breadth of the proximal end	von den Driesch 1976
	BFp	Greatest breadth of the *facies articularis proximalis*	von den Driesch 1976
	Dp	Greatest depth of the proximal end (only when the ulna is not attached to the radius)	Salvagno and Albarella 2017, adapted from Fernández 2001's DAPpA-DAPpM
+	V	Medial height of the insertion for the lateral ulnar articulation for the radius (red deer and fallow deer only; only when the ulna is not attached to the radius; taken with the caliper upper jaws)	OR1 Fig. 4
tibia	GL	Greatest length	von den Driesch 1976
	SD	Smallest breadth of the diaphysis	von den Driesch 1976
+	*SD1*	Smallest depth of the diaphysis	OR1 Fig. 8
	Bd	Greatest breadth of the distal end	von den Driesch 1976
	Dda	Depth of the distal end on the medial side	Salvagno and Albarella 2017, renamed after von den Driesch 1976
	Ddb	Depth of the distal end on the lateral side	Salvagno and Albarella 2017
astragalus	GLl	Greatest length of the lateral half	von den Driesch 1976
	GLm	Greatest length of the medial half	von den Driesch 1976
	H	Height of the central constriction (i.e., minimum length)	Salvagno and Albarella 2017
	Dl	Greatest depth of the lateral half	von den Driesch 1976
	Bd	Greatest breadth of the distal end	von den Driesch 1976
calcaneum	*c*	Length of the articular facet of the *os malleolare*	Fernández 2001
	d	Length from the distal end of the articular facet of the *os malleolare* to the end of the proximal end of the calcaneum. Adapted from S&A, where the measurement is taken from where the articular facet starts projecting out	adapted from Salvagno and Albarella 2017
	B	Breadth of the articular surface of the *os malleolare*	Boessneck et al. 1964
+	Bd	Greatest breadth of the distal end	OR1 Fig. 6
+	Dd	Greatest depth of the distal end, taken with the caliper jaws parallel to the dorsal crest	OR1 Fig. 7
metapodials	GL	Greatest length	von den Driesch 1976
	Bp	Greatest breadth of the proximal end	von den Driesch 1976
	Dp	Greatest depth of the proximal end	von den Driesch 1976
	SD	Smallest breadth of the diaphysis	von den Driesch 1976
+	*SD1*	Smallest depth of the diaphysis	OR1 Fig. 8
	BFd	Breadth of the distal articular facet	Davis 1996
	a or WCM	Medio-lateral width of the medial condyle taken in the middle	Payne 1969; Davis 1996
	b or WCL	Medio-lateral width of the lateral condyle taken in the middle	Payne 1969; Davis 1996

Table 2 (continued)

Element	Measurement	Description	Reference(s)
	1 or DEM	Antero-posterior diameter of the external trochlea of the medial condyle, taken at its constriction	Payne 1969; Davis 1996
	2 or DVM	Antero-posterior diameter of the verticillus of the medial condyle	Davis 1996
	3 or DIM	Antero-posterior diameter of the internal trochlea of the medial condyle	Davis 1996
	4 or DEL	Antero-posterior diameter of the external trochlea of the lateral condyle, taken at its constriction	Payne 1969; Davis 1996
	5 or DVL	Antero-posterior diameter of the verticillus of the lateral condyle	Davis 1996
	6 or DIL	Antero-posterior diameter of the internal trochlea of the lateral condyle	Davis 1996

providing a baseline on which to plot values from archaeological specimens; a similar approach can be found in methodological works focussing on other animal taxa, such as Payne (1969), Tomek and Bocheński (2009), Salvagno and Albarella (2017), and Poland (2018).

The assessment of distribution and degree of separation of values from the three species primarily relied on data visualisation using scatterplots, often combining size ranges and shape indices (e.g., distal tibia: Bd *vs* Ddb/Dda); this approach aims to optimise the separation potentials of dimensional and morphological differences. For most zones, scatter plots with shape indices only are also presented, in order to offer additional evidence from morphological analyses. The results are summarized by presenting the shape index value means for each element and species, displayed in a linear graph and expressed as Logarithmic Size Index (LSI) values using the red deer means as the standard; LSI, like other size index scaling techniques, compares each value (in this case, those of shape indices) to a standard one (here, the red deer mean values), thus producing relative values that can be compared on the same scale (Meadow 1999; Albarella 2002). The values of each shape index are also displayed in notched box plots, further describing and comparing the value distributions of the three species (Online Resource 3).

The groups of shape index values were statistically tested using the software R; statistical tests were performed using the R *prcomp* function (R Core Team 2025). In detail, the statistical significance of differences between shape index values were calculated for comparisons of fallow deer with red deer and roe deer; both the Mann–Whitney U test and the Student's t-test of significance were used. The resulting *p*-values are reported in tables; for each element, the *p*-values are also displayed graphically (Online Resource 4), providing a complementary visual summary.

The Principle Component Analysis (PCA) was run for specific element zones using shape indices (Table 3), to provide an additional assessment of morphological differences among red deer, fallow deer, and roe deer. The exclusion of absolute size data from the PCA analyses ensured that the latter focused exclusively on morphology, rather than giving precedence to the more straightforward, but often insufficient separation potential offered by size; such analyses were conducted on mature specimens only, with the exception of the articular end of the calcaneum, for which separate analyses were performed on mature and immature specimens. PCA is an unsupervised data reduction technique, capturing the maximum variance without using class labels in the computation. For each zone, it reduced all shape indices to two dimensions (PC1, PC2), that provided the best separation of the three cervid species. Multivariate outliers were identified and removed using the Mahalanobis distance method with a threshold of 0.975 (i.e., $p < 0.025$); this method measures data points' distance from the multivariate centre while accounting for correlations between variables. PCA was performed using the R *prcomp* function (R Core Team 2025), defined in the *stats* package (version 3.6.2); results were visualized with ggplot2 (version 3.5.2; Wickham et al. 2025) and are presented in Online Resource 5.

Results

Scapula

The size ranges of the greatest length of the *processus articularis* (GLP; Fig. 4, graph A) show partial overlap between fallow deer and red deer, particularly in the 42–48 mm range. This overlap indicates that, in this case, size alone can be insufficient for reliable species identification. By contrast, roe deer forms a distinct cluster of smaller values, clearly separated from those of fallow deer and red deer. The shape index ASG/GLP offers good morphological separation of fallow and red deer: fallow deer exhibits lower values, suggesting that this species' scapulae have a proportionally shorter distance between the base of the spine and the edge of the glenoid cavity compared to red deer and roe deer. In fallow deer and red deer, there also seems to exist a negative allometry whereby larger specimens tend to have lower index values; such allometries follow different regression lines, favouring separation of the two species.

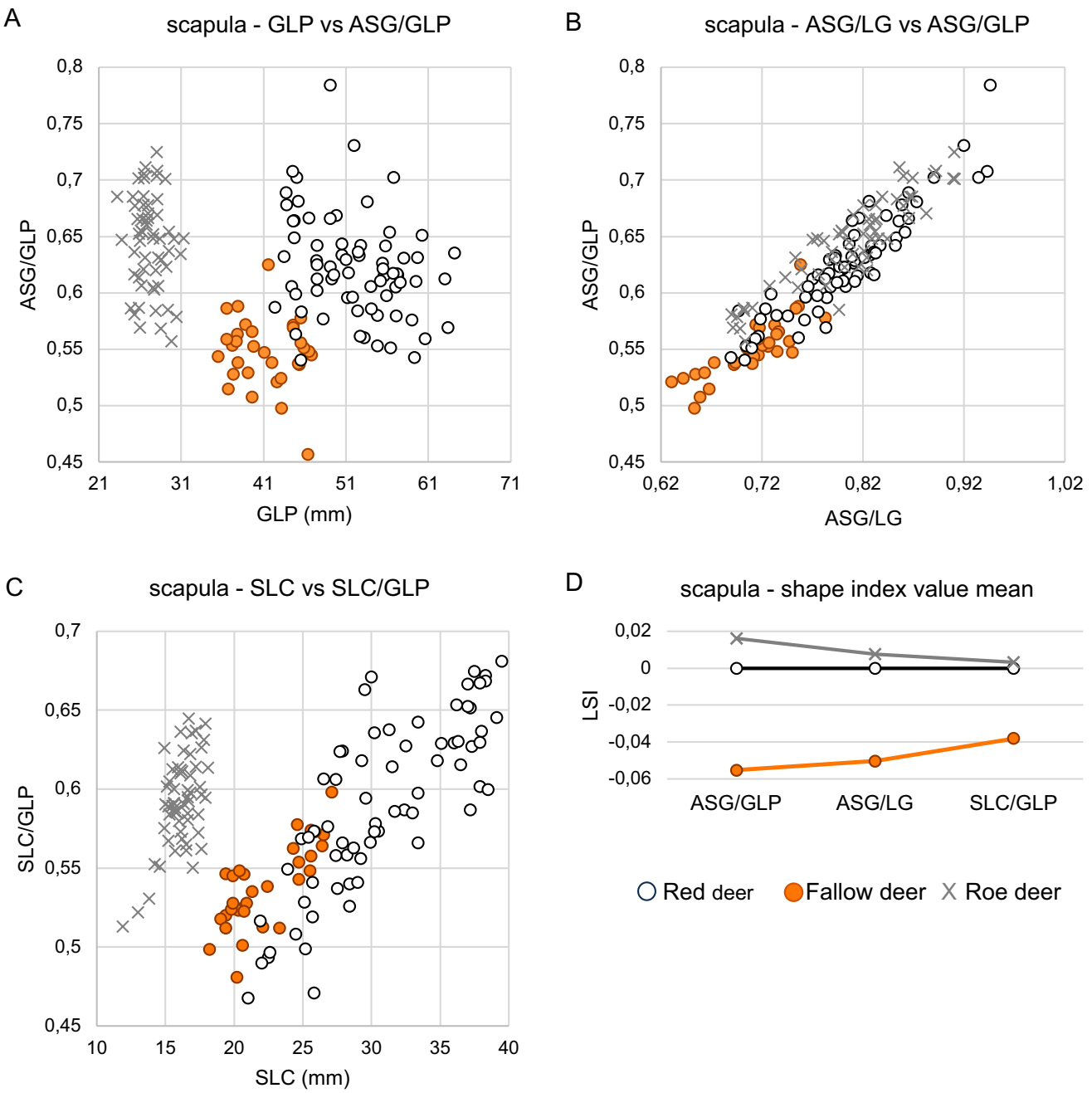

Fig. 4 Size and shape index ranges for the scapula. **A**. GLP vs ASG/GLP; **B**. ASG/LG vs ASG/GLP; **C**. SLC vs SLC/GLP. The means of shape index values (**D**) from the three species are expressed as LSI values, using the mean values of red deer indices as the standard (box plots for the shape indices analysed in this study are available in Online Resource 3: Fig. 1)

In graph B, the same index is plotted against ASG/LG, resulting in a partial isolation of fallow deer values in the bottom-left part of the graph.

In graph C, the smallest length of the collum scapulae (SLC) is plotted against its ratio to GLP. Fallow deer and red deer distributions show a positive allometry, a consequence of the fact that SLC size increase with age is greater than in other measurements; however, the former species presents lower SLC/GLP values, suggesting that the collum scapulae of fallow deer is proportionally narrower relative to the length of the *processus articularis*.

The shape index value means in graph E summarise well the observations made above, highlighting the extent to which different indices allow to isolate fallow deer specimens; the results of statistical tests fully support such separation potentials (Table 3). Also the results of the PCA confirm the good separation provided by biometric analyses for fallow deer specimens (Online Resource 5: Fig. 1).

Table 3 *p*-values from Mann–Whitney U tests (MWU) and Student's t-test (St) for the shape indices of the scapula. A graphical representation of the results is available in Online Resource 4: Fig. 1

Mann–Whitney U test and Student's t-test: *p*-values				
Shape index	Fallow-red deer		Fallow-roe deer	
	MWU	St	MWU	St
ASG/LG	<0.001	<0.001	<0.001	<0.001
ASG/GLP	<0.001	<0.001	<0.001	<0.001
SLC/GLP	<0.001	<0.001	<0.001	<0.001
BG/LG	0.002	0.001	0.039	0.014

Humerus

In Fig. 5, graph A highlights some degree of overlap of Bd fallow deer and red deer values; HX/Bd values, however, tend to be lower in fallow deer, ensuring almost complete separation of the two clusters. Such lower values compared to red deer may reflect the separation criterion presented in Di Stefano (1995: Fig. 5 therein), where it is suggested that, in fallow deer, the trochlea is directed laterally with a more acute angle. There is also a clear negative allometric relation between size and the shape index, at least in fallow deer and red deer, although such allometries rely on different regression lines. In graph B, two other shape indices (HTL/BT and HTL/Bd) separate well fallow deer and roe deer, as the two species present respectively the lowest and highest values in both indices; red deer values lie in between, therefore partly overlapping with fallow deer values. As both indices involve the diameter of the capitulum (HTL), it seems that this latter is, on average, proportionally smaller in fallow deer. The same explanation may apply to the lower HTL/HTC index values of fallow deer in graph C, which allow to overcome the only slight HTC size overlap with red deer. Two other shape indices employing distal end height measurement values (HTC/HX and HTL/HX) provide mild separation of fallow deer values from red deer and roe deer ones (graph D).

Shape indices combining shaft and distal end measurements (graph E, SD/HTC vs SD1/HTC), and the combined plotting of shape indices of the shaft and distal widths (graph F, SD1/SD vs BT/Bd) provide the best morphological separations, although in the latter graph this applies to the separation of fallow deer and red deer specimens only.

The smallest breadth of the shaft (SD) highlights a significant size overlap between fallow deer and red deer specimens but the fallow deer shape index (SD1/SD) values plot lower (graph G), indicating that this species' humerus shaft is more tubular while the red deer's is more projecting antero-posteriorly. To some extent, this characteristic applies to immature specimens as well (graph H), where size overlap is substantial; however, there seems to be a positive allometry along similar regression lines in fallow deer and red deer, which may compromise the effectiveness of morphological separation.

In mature specimens, the greatest length from the caput (GLC) values displays substantial dimensional overlap between fallow deer and roe deer and, to a smaller extent, between fallow deer and red deer (graph I). Both graphs I and J highlight the greater slenderness of roe deer humeri, whose shape index values plot on the bottom-left area of the graphs. Fallow deer and red deer shape index values are also well separated; in graph I, this is probably the result of the capitulum being proportionally smaller in fallow deer (as seen in graphs B, C), while in graph J such separation reflects the different proportion between shaft measurements (as seen in graphs F–H).

The shape index value means (graph K) broadly support the observations made for graphs A-J. The overall slenderness shape indices see the fallow deer closer to the red deer, as do many of the distal end indices though with useful exceptions. Shaft morphology, on the other hand, differentiates to a good degree red deer from the two smaller species, as do most shape indices combining shaft and distal end measurements. The results of statistical tests for the shape index measurements support the observations above (Table 4). The results of the PCA reflect well both the partial separation of fallow deer and red deer specimens, and the greater isolation of roe deer (Online Resource 5: Fig. 2).

Radius

The value range of Bp indicates some dimensional overlap between fallow deer and red deer values, while roe deer values separate well from fallow deer's (Fig. 6, graph A). The BFp/Bp shape index values of fallow deer are on average lower compared to red deer's, reflecting a more pronounced lateral bicipital tuberosity in the former species and ensuring complete separation of the two clusters; in addition, biometrical data from both species reveal a negative allometric relation between size and the shape index values, although following different regression lines and thus favouring species separation. BFp values also show some dimensional overlap between the two larger species but the shape index V/BFp produces lower values for the fallow deer, as the insertion for the lateral ulnar articulation is often less pronounced in this species (graph B) – possibly a reflection of character 6 from Lister (1996: Fig. 2, Part 4 therein). The shape indices employing the proximal depth and widths present substantial overlaps, but fallow deer values run partly parallel to red deer's and roe deer's (graph C).

The proportions between the smallest depth of the shaft (located close to the proximal end) and the proximal widths display a wider range of values for the red deer relative to the fallow deer, that does not seem driven only by differences

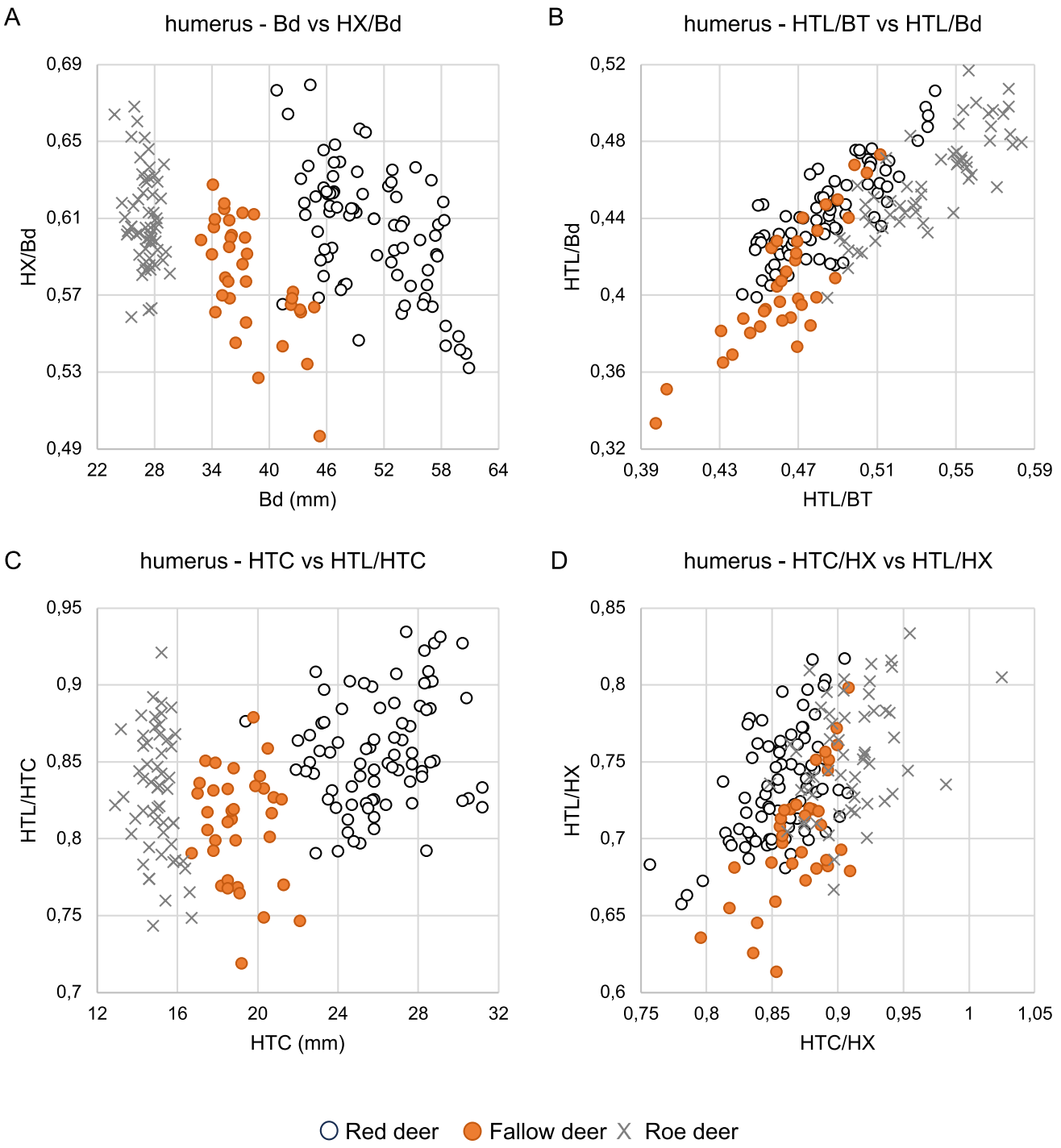

Fig. 5 Size and shape index ranges for the humerus. For the distal end: **A**. Bd vs HX/Bd; **B**. HTL/BT vs HTL/Bd; **C**. HTC vs HTL/HTC; **D**. HTC/HX vs HTL/HX. Graphs **E** (SD/HTC vs SD1/HTC), **F** (SD1/SD vs BT/Bd) combine distal end and shaft measurements. For the shaft: SD vs SD1/SD for adult (**G**) and immature (**H**) specimens. For overall proportions of complete mature humeri: **I**. GLC vs HTL/GLC; **J**. SD/GLC vs SD1/GLC. The means of shape index values (**K**) from the three species are expressed as LSI values, using the mean values of red deer indices as the standard; for the shaft shape index, the means of immature specimens (proximal end unfused, distal end unfused, fusing or fused) are also presented (IM.: immature; box plots for the shape indices analysed in this study are available in Online Resource 3: Fig. 2)

in sample size, while they provide some separation between the two smaller species (graph D). Similarly, the shaft shape index (SD/SD1) does not separate fallow deer and red deer, which also present substantial size overlap, but provides some mild separation between fallow and roe deer (graph E).

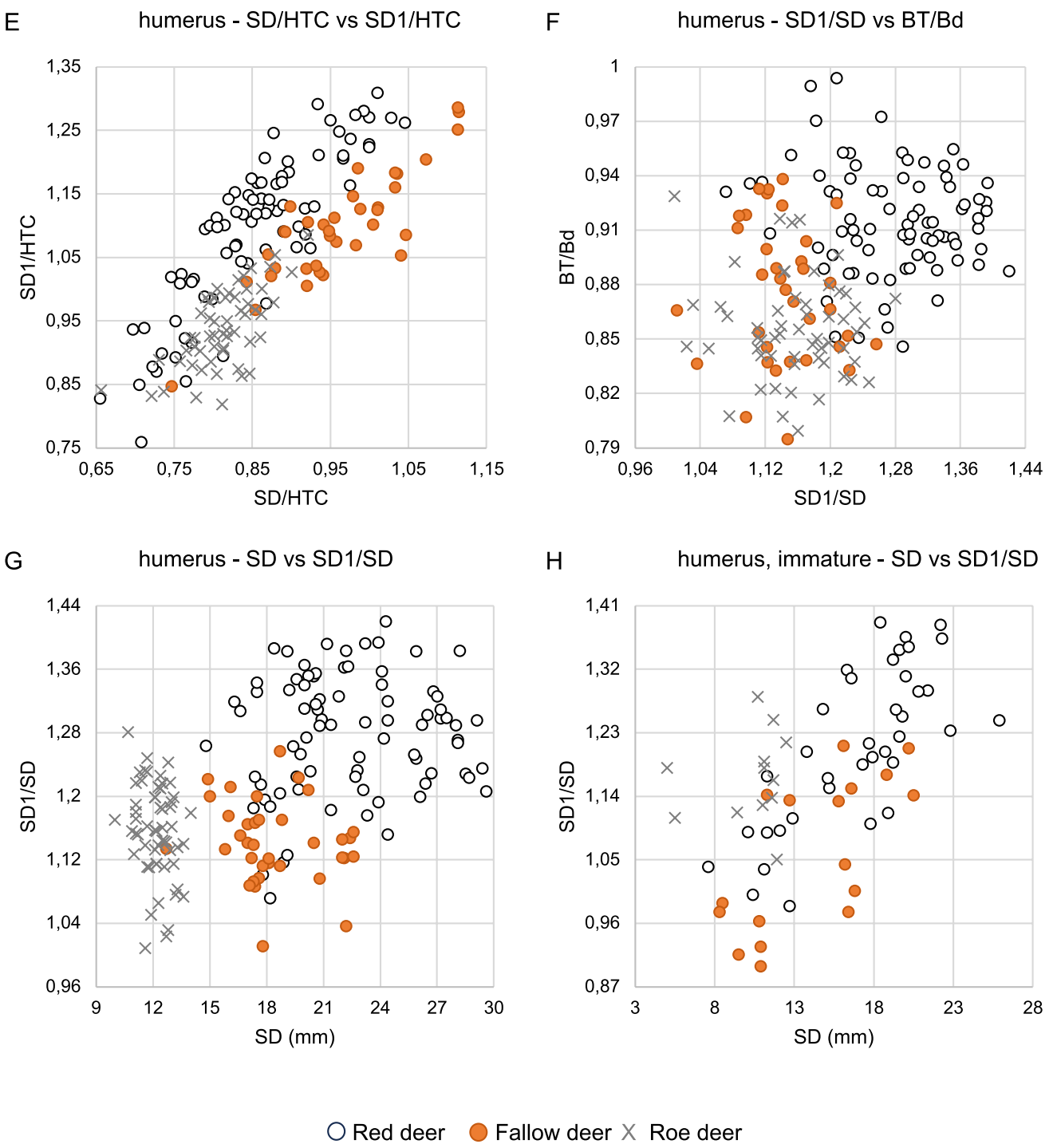

Fig. 5 (continued)

In mature specimens (both ends' epiphyses fused or fusing), the robustness index SD/GL efficiently describes the greater slenderness of roe deer radii, separating them well from the cluster of fallow deer values despite a substantial size overlap; fallow deer and red deer values are well separated by size as well as by positive allometries along different regression lines (graph F).

The shape index value means (graph G) broadly support the observations made for graphs A-F. Most indices highlight substantial morphological similarities between fallow deer and red deer, with the important exceptions of all indices involving measurement V and, to a lesser extent, of indices employing BFp. Roe deer, on the other hand, separates well from the fallow deer, displaying a

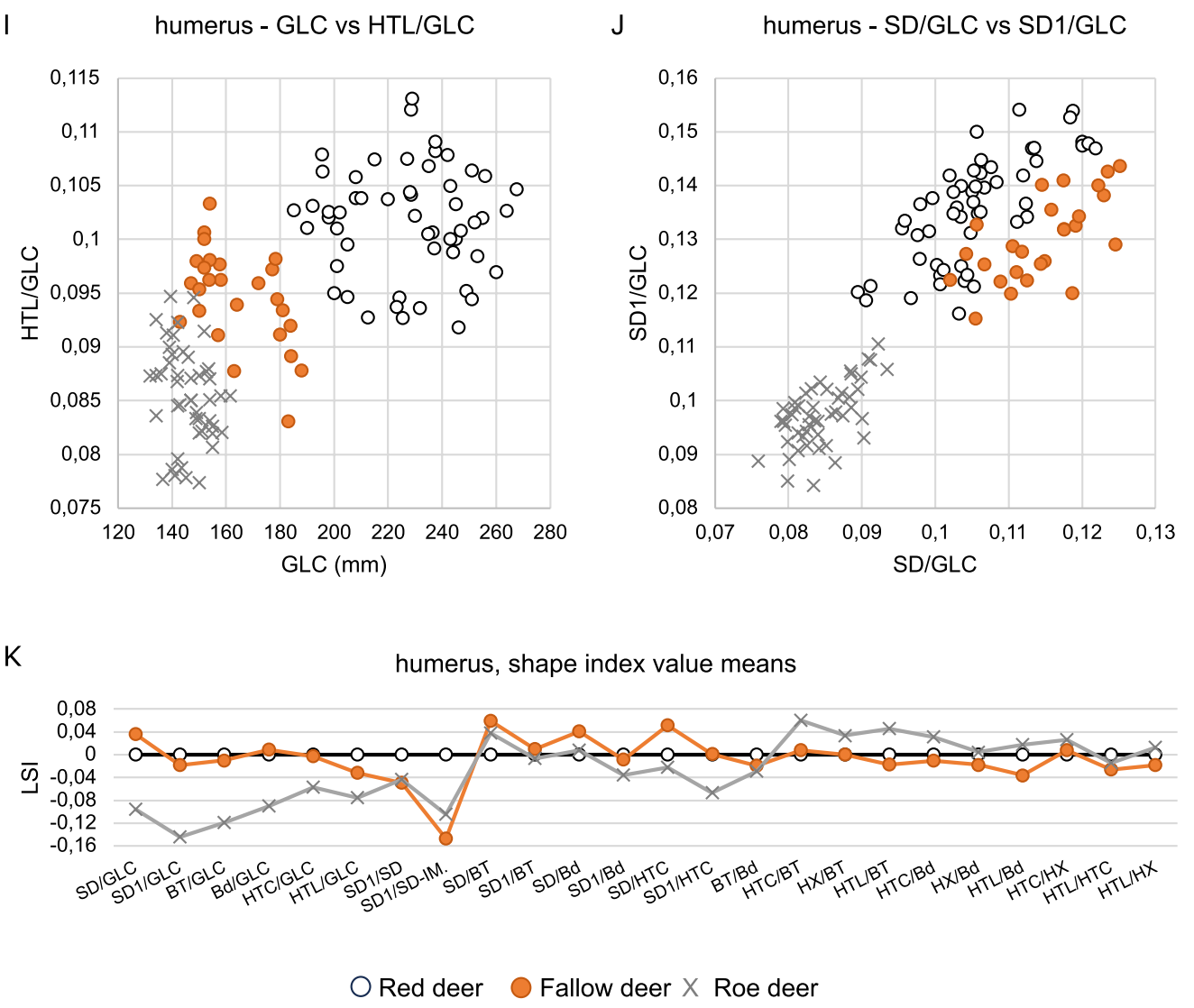

Fig. 5 (continued)

Table 4 *p*-values from Mann–Whitney U tests (MWU) and Student's t-test (St) for the shape indices of the humerus. A graphical representation of the results is available in Online Resource 4: Fig. 2

Mann–Whitney U test and Student's t-test: *p*-values									
Shape index	Fallow-red deer		Fallow-roe deer		Shape index	Fallow-red deer		Fallow-roe deer	
	MWU	St	MWU	St		MWU	St	MWU	St
SD/GLC	<0.001	<0.001	<0.001	<0.001	SD/HTC	<0.001	<0.001	<0.001	<0.001
SD1/GLC	0.021	0.008	<0.001	<0.001	SD1/HTC	0.606	0.890	<0.001	<0.001
BT/GLC	0.003	0.001	<0.001	<0.001	BT/Bd	<0.001	<0.001	0.014	0.010
Bd/GLC	0.714	0.679	<0.001	<0.001	HTC/BT	0.019	0.010	<0.001	<0.001
HTC/GLC	0.443	0.646	<0.001	<0.001	HX/BT	0.738	0.960	<0.001	<0.001
HTL/GLC	<0.001	<0.001	<0.001	<0.001	HTL/BT	0.001	<0.001	<0.001	<0.001
SD1/SD	<0.001	<0.001	0.146	0.210	HTC/Bd	0.026	0.027	<0.001	<0.001
SD1/SD-IM	<0.001	<0.001	0.014	0.002	HX/Bd	<0.001	<0.001	<0.001	<0.001
SD/BT	<0.001	<0.001	<0.001	0.002	HTL/Bd	<0.001	<0.001	<0.001	<0.001
SD1/BT	0.417	0.233	0.015	0.026	HTC/HX	0.005	0.010	<0.001	<0.001
SD/Bd	<0.001	<0.001	<0.001	<0.001	HTL/HTC	<0.001	<0.001	0.013	0.007
SD1/Bd	0.092	0.287	<0.001	<0.001	HTL/HX	<0.001	<0.001	<0.001	<0.001

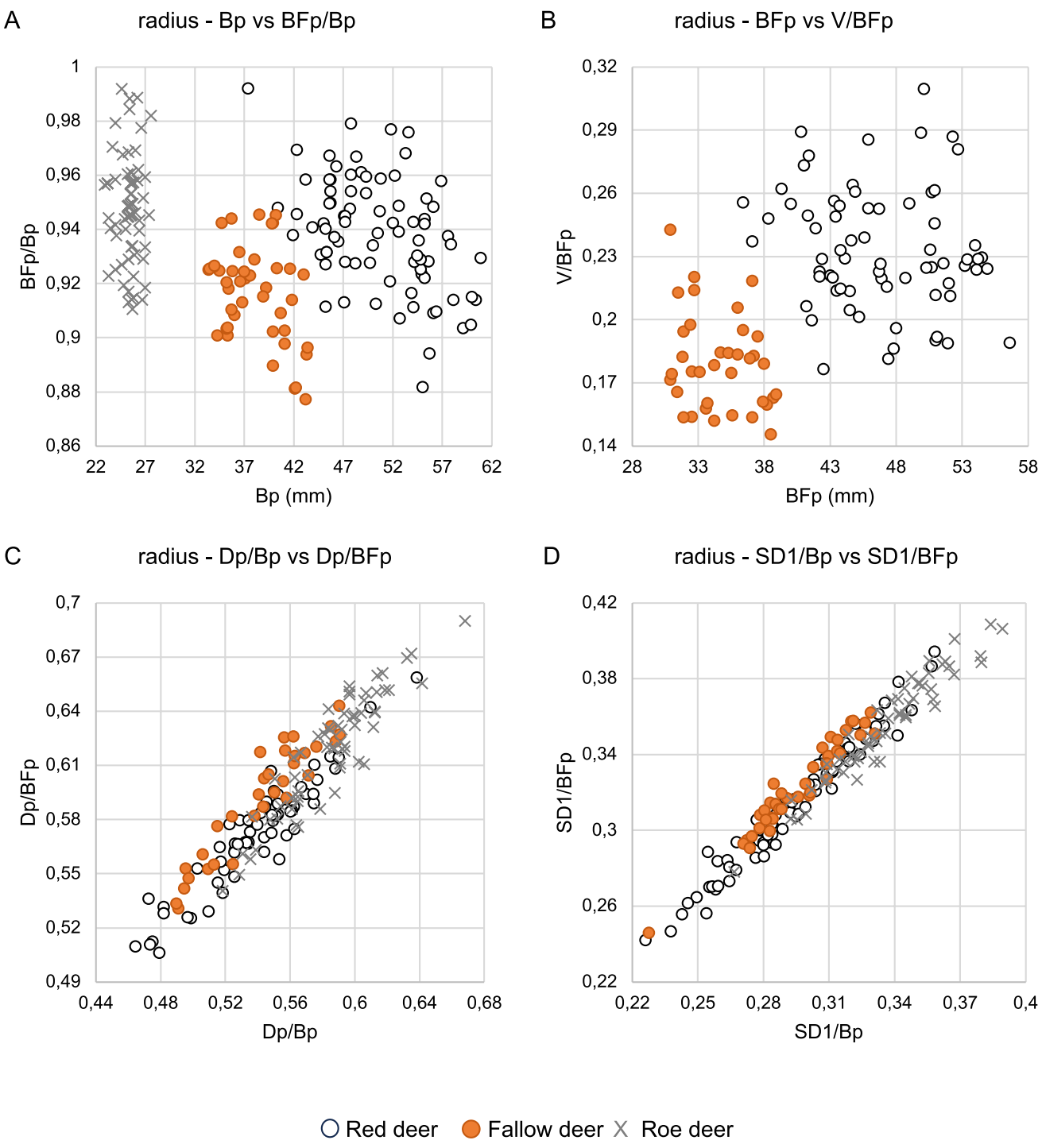

Fig. 6 Size and shape index ranges for the radius. For the proximal end: **A**. Bp vs BFp/Bp; **B**. BFp vs V/BFp; **C**. Dp/Bp vs Dp/BFp. Graph **D** (SD1/Bp vs SD1/BFp) combines distal end and shaft measurements. For the shaft: **E**. SD vs SD1/SD for mature specimens. For overall proportions of complete mature radii: **F**. GL vs SD/GL. The means of shape index values (**G**) from the three species are expressed as LSI values, using the mean values of red deer indices as the standard; for the shaft shape index, the means of immature specimens (proximal end unfused, distal end unfused, fusing or fused) are also presented (IM.: immature; box plots for the shape indices analysed in this study are available in Online Resource 3: Fig. 3)

greater overall slenderness and different average values for most proximal end and shaft indices. The results of statistical tests for the shape index measurements support the observations above (Table 5). The results of the PCA highlight the partial separation of fallow deer from red and roe deer, as well as the efficiency of shape indices using

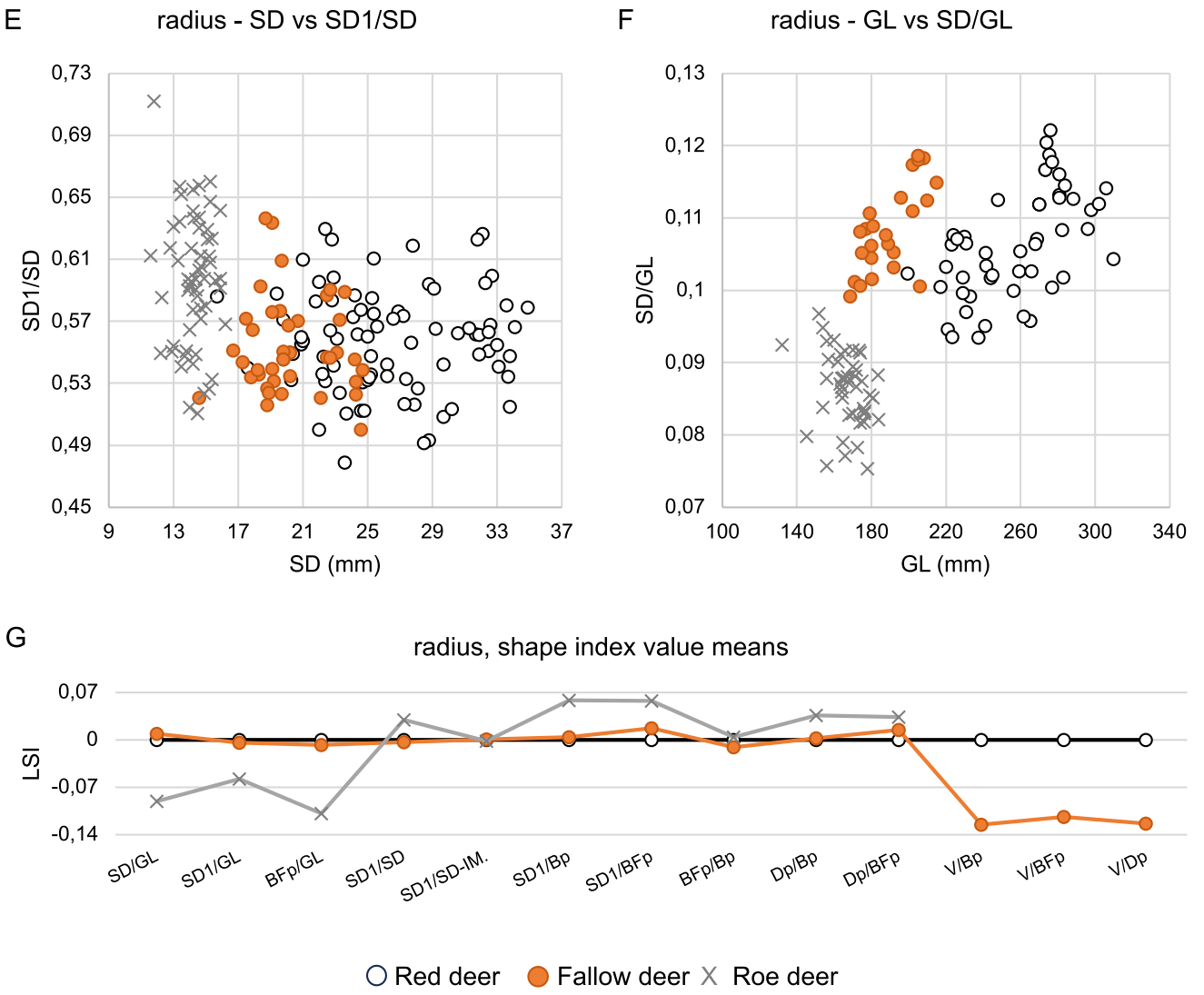

Fig. 6 (continued)

Table 5 *p*-values from Mann–Whitney U tests (MWU) and Student's t-test (St) for the shape indices of the radius. A graphical representation of the results is available in Online Resource 4: Fig. 3

Mann–Whitney U test and Student's t-test: *p*-values				
Shape index	Fallow-red deer		Fallow-roe deer	
	MWU	St	MWU	St
SD/GL	0.206	0.161	<0.001	<0.001
SD1/GL	0.822	0.617	<0.001	<0.001
BFp/GL	0.047	0.022	<0.001	<0.001
SD1/SD	0.347	0.538	<0.001	<0.001
SD1/SD-IM	0.853	0.969	0.654	0.921
SD1/Bp	0.463	0.516	<0.001	<0.001
SD1/BFp	0.018	0.020	<0.001	<0.001
BFp/Bp	<0.001	<0.001	<0.001	<0.001
Dp/Bp	0.552	0.619	<0.001	<0.001
Dp/BFp	0.003	0.005	<0.001	<0.001
V/Bp	<0.001	<0.001	-	-
V/BFp	<0.001	<0.001	-	-
V/Dp	<0.001	<0.001	-	-

measurement V in separating fallow and red deer (Online Resource 5: Figs. 3, and 4).

Metacarpus

Biometric data show no substantial dimensional overlap in the absolute values of measurement a among the three species, only fallow deer and red deer values slightly overlapping in the range 14–16 mm; the shape index a/2 maximises the separation of the three clusters as the fallow deer index presents higher values (Fig. 7, graph A). In both the fallow deer and the red deer, there seems to be a positive allometric relation between size and the shape index used, although along different regression lines. Two shape indices from the medial condyle, a/3 and 3/2 (graph B), also perform well in separating the three species: the resulting distribution assumes a clover-shaped pattern, with only partial overlap

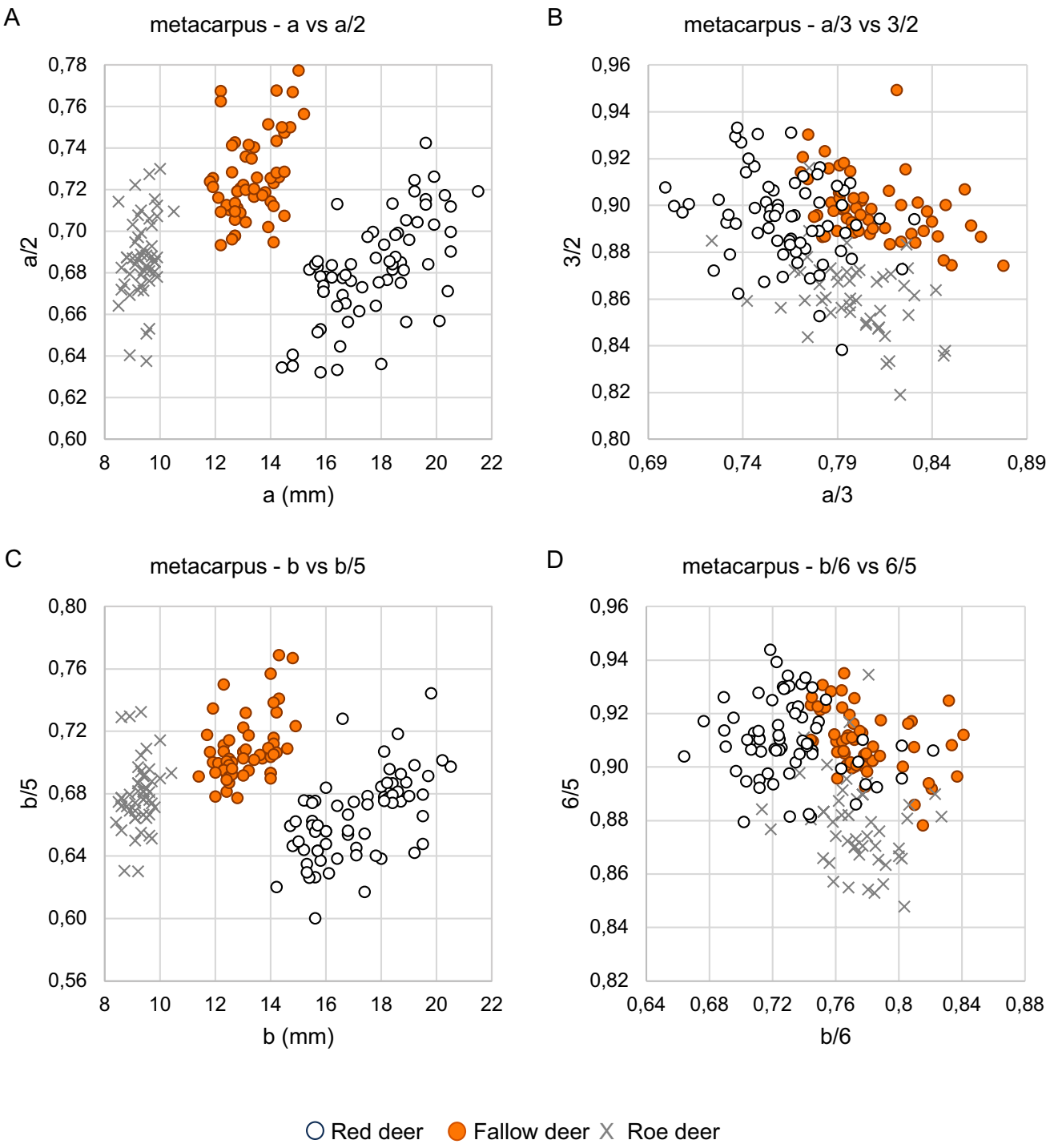

Fig. 7 Size and shape index ranges for the metacarpus. For the distal end: **A**. a vs a/2; **B**. a/3 vs 3/2; **C**. b vs b/5; **D**. b/6 vs 6/5; **E**. a/Bd vs b/Bd. Graph **F** combines distal end and shaft measurements. For the shaft: SD vs SD1/SD for adult (**G**) and immature (**H**) specimens. For overall proportions of complete mature metatarsi: GL vs SD/GL (**I**) and SD1/GL vs Bd/GL (**J**). The means of shape index values (**K**) from the three species are expressed as LSI values, using the mean values of red deer indices as the standard (IM.: immature; box plots for the shape indices analysed in this study are available in Online Resource 3: Fig. 4)

of red deer and fallow deer values, thus reinforcing the diagnostic value of the medial condyle's biometric proportions.

In graph C, measurement b shows a similarly low degree of dimensional overlap between fallow deer and red deer, while the shape index b/5 enhances cluster separation, particularly between the two larger species; similar allometric relations to those in graph A are observed. Despite a slightly higher degree of overlap between fallow and red

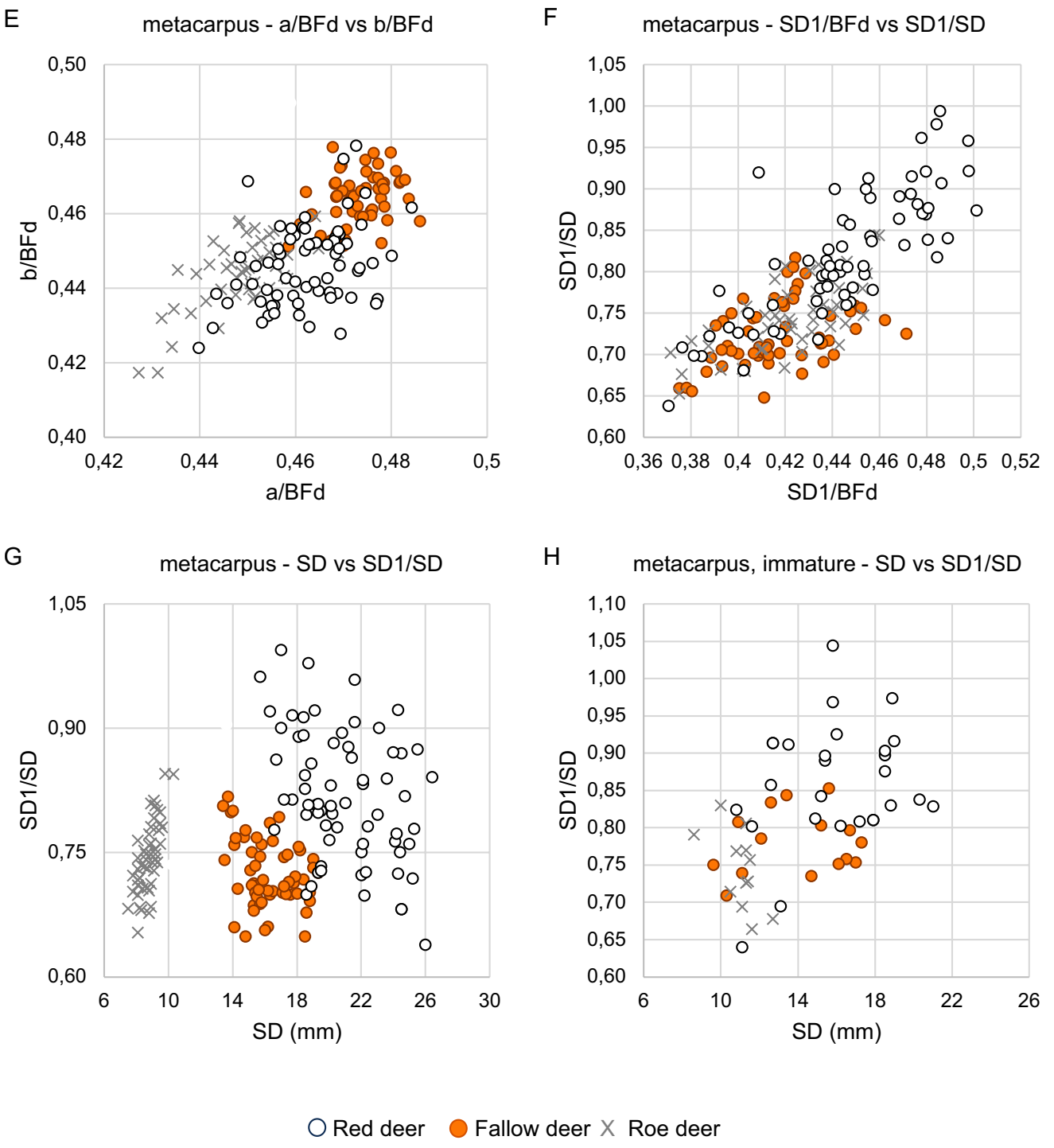

Fig. 7 (continued)

deer, the b/6 and 6/5 shape indices still provide good separation of the three taxa (graph D). Overall, distal widths of the metacarpus in fallow deer are proportionally less reduced relative to depths than in red deer and roe deer. In addition, the roe deer exhibits more pronounced proportional differences between the antero-posterior diameters of the verticillus and of the internal trochlea compared to the two larger species. Similar results were also obtained for the metatarsus.

Proportions between condylar widths and the total width of the distal articular facet are assessed in graph E. Despite some overlap, fallow deer values tend to cluster in the top-right part of the graph, suggesting the condyles of this species are less spaced. Shape indices related to shaft

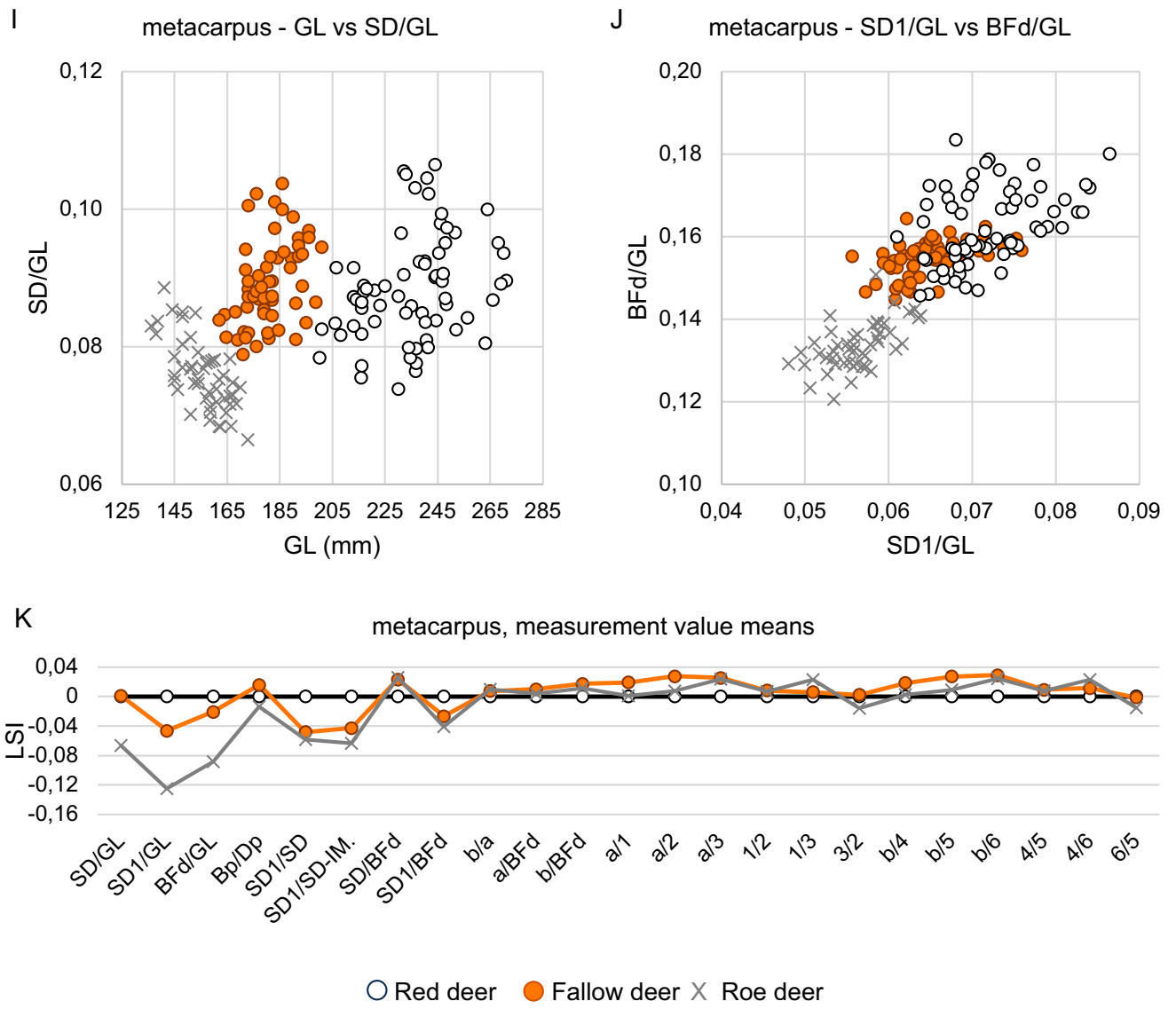

Fig. 7 (continued)

morphology, particularly SD1/BFd and SD1/SD, indicate that fallow deer (and roe deer) has a proportionally flatter shaft compared to red deer (graph F). This pattern is consistent with findings from other postcranial elements, pointing to a characteristically flatter shaft profile in fallow deer.

When the smallest breadth of the shaft (SD) is plotted against the shaft index SD1/SD (graph G), size overlap between fallow and red deer is substantial, but the two species are well separated by the combination of size and shape analyses. Similar observations can be made for immature specimens (graph H), where fallow deer continues to display lower shaft index values.

In mature specimens, greatest length (GL) values for the metacarpus (graph I) show almost no dimensional overlap between fallow and red deer, and a much greater degree of overlap between roe deer and fallow deer; however, shape indices incorporating GL—such as SD/GL, SD1/GL, and BFd/GL (graphs I and J)—highlight the consistently greater slenderness of roe deer metacarpi. In addition, graph I indicates a negative allometric relation between roe deer metacarpus length and slenderness.

In graph J, also the fallow deer separates relatively well from the red deer.

The mean values of shape indices across species (graph K) summarise well the trends observed in the scatter plots. In detail, indices involving shaft measurements highlight the greater flatness of fallow deer bones, as do those describing condylar morphology, while roe deer bones are more slender. The results of statistical tests support the separation potentials of most indices (Table 6). Also the results of the PCA confirm the excellent degree of separation of red deer,

Table 6 *p*-values from Mann–Whitney U tests (MWU) and Student's t-test (St) for the shape indices of the metacarpus. A graphical representation of the results is available in Online Resource 4: Fig. 4

Mann–Whitney U test and Student's t-test: *p*-values									
Shape index	Fallow-red deer		Fallow-roe deer		Shape index	Fallow-red deer		Fallow-roe deer	
	MWU	St	MWU	St		MWU	St	MWU	St
SD/GL	0.658	0.836	<0.001	<0.001	a/2	<0.001	<0.001	<0.001	<0.001
SD1/GL	<0.001	<0.001	<0.001	<0.001	a/3	<0.001	<0.001	0.159	0.764
BFd/GL	<0.001	<0.001	<0.001	<0.001	1/2	<0.001	<0.001	0.846	0.482
Bp/Dp	<0.001	<0.001	<0.001	<0.001	1/3	<0.001	0.001	<0.001	<0.001
SD1/SD	<0.001	<0.001	<0.001	0.168	3/2	0.277	0.124	<0.001	<0.001
SD1/SD-IM	<0.001	<0.001	0.092	0.066	b/4	<0.001	<0.001	<0.001	<0.001
SD/BFd	<0.001	<0.001	0.208	0.765	b/5	<0.001	<0.001	<0.001	<0.001
SD1/BFd	<0.001	<0.001	0.271	0.466	b/6	<0.001	<0.001	0.843	0.181
b/a	<0.001	<0.001	0.006	0.244	4/5	<0.001	0.001	0.858	0.525
a/BFd	<0.001	<0.001	<0.001	0.708	4/6	<0.001	0.013	<0.001	0.019
b/BFd	<0.001	<0.001	<0.001	0.626	6/5	0.883	0.443	<0.001	<0.001
a/1	<0.001	<0.001	<0.001	<0.001					

fallow deer, and roe deer specimens (Online Resource 5: Fig. 5).

Tibia

The size values of the distal breadth of the tibia (Fig. 8, graph A) display limited overlaps between fallow deer and red deer in the range 36–38 mm. The shape index Ddb/Dda (i.e., the proportion between the medial and lateral distal depths) separates well the fallow deer from the red and roe deer, although with some overlap between the two larger species. This separation indicates that the difference between the two depths is proportionally greater in fallow deer, although values from red deer and fallow deer seem distributed according to a positive allometric relation along similar regression lines, potentially compromising the diagnostic potentials of this shape index.

Differences in the proportions of the tibia distal end measurement values are also visible in the shape indices of graph B, where both the proportions between the distal breadth and the two depths contribute to separate well the fallow deer from the two other cervids. The fallow deer shape index values run parallel to those of red deer and roe deer, indicating that in this species the medial depth is proportionally greater, and the lateral one proportionally smaller, than the distal breadth.

In graph C, the smallest breadth of the shaft (SD) displays a much greater degree of size overlap between fallow deer and red deer values, the former species mostly plotting with the smaller third of the latter species. The proportion between the shaft breadth and depth (shape index SD1/SD), however, separates well the fallow deer from the roe and red deer. The shape index values of the first species plot lower, indicating that the fallow deer tibia shaft is consistently 'flatter' than that of the other two species; the proportionally larger breadth of the shaft in fallow deer also explains the considerable size overlap with red deer values. In addition, fallow deer and red deer values seem characterised by negative allometric relations along different regression lines. The same shape index also works on immature specimens (graph D), where fallow deer size values can overlap with both red and roe deer ones.

Although complete adult long bones are rarely recovered from archaeological contexts, graph E shows that roe deer tibiae are overall much more slender than those of the other cervids. SD being proportionally larger in fallow deer (graphs C, D) also provides some mild separation between this species and red deer, though with considerable overlap.

The shape index value means (graph F), calculated as LSI values using the red deer means as standard, well describe the observations made for graphs A-E. The results of statistical tests for the shape index measurements fully support the observations above (Table 7). Also the results of the PCA confirm the good degree of separation provided by biometric analyses for the three species (Online Resource 5: Fig. 6).

Astragalus

The size and shape index range analyses for the astragalus focus on fully ossified specimens only. The size ranges display some dimensional overlap between fallow deer and red deer values, while roe deer values are, as usual, better detached from those of the larger species. Both the shape indices GLm/GLl and Bd/H provide very little separation of fallow deer and red deer values, the latter plotting slightly lower, while the shape index values of the two smaller species overlap (Fig. 9, graphs A, B). Graph B, however, highlights negative allometric relations between size and the values of the shape index of fallow deer and red

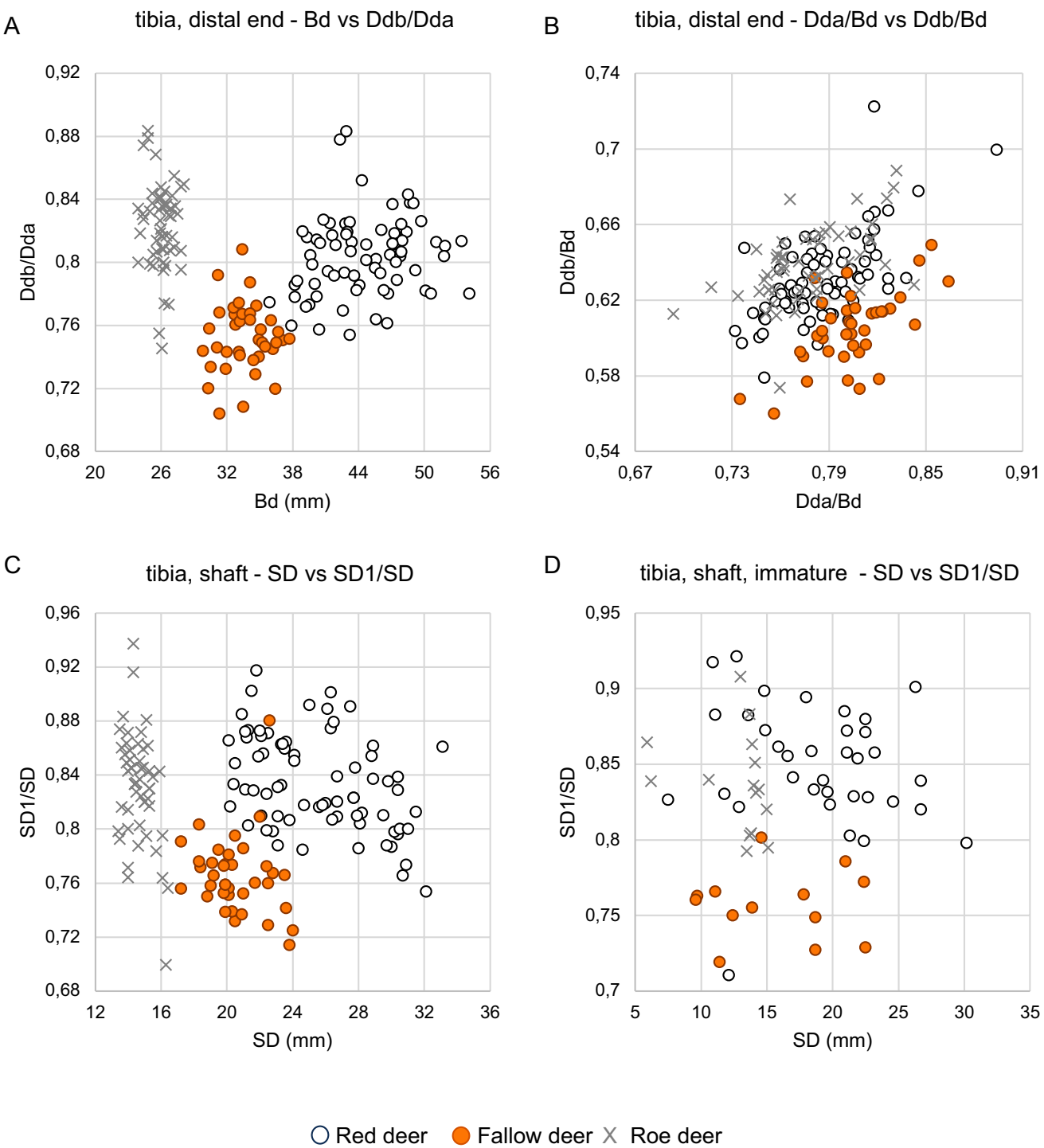

Fig. 8 Size and shape index ranges for the tibia. For the distal end: **A**. Bd vs Ddb/Dda; **B**. Dda/Bd vs Ddb/Bd. For the shaft: SD vs SD1/SD for adult (**C**) and immature (**D**) specimens. For overall proportions of complete mature tibiae: SD/GL vs Bd/GL (**E**). The means of shape index values (**F**) from the three species are expressed as LSI values, using the mean values of red deer indices as the standard (IM.: immature; box plots for the shape indices analysed in this study are available in Online Resource 3: Fig. 5)

deer, following different regression lines and thus possibly enhancing species separation potentials.

In graph C, two other shape indices display substantial overlap of values from the three species but with the red deer cluster slightly skewed towards the bottom-left of the graph compared to fallow deer's. The shape index value means (graph D) reflect these slightly different dimensional proportions between red deer specimens and the two other

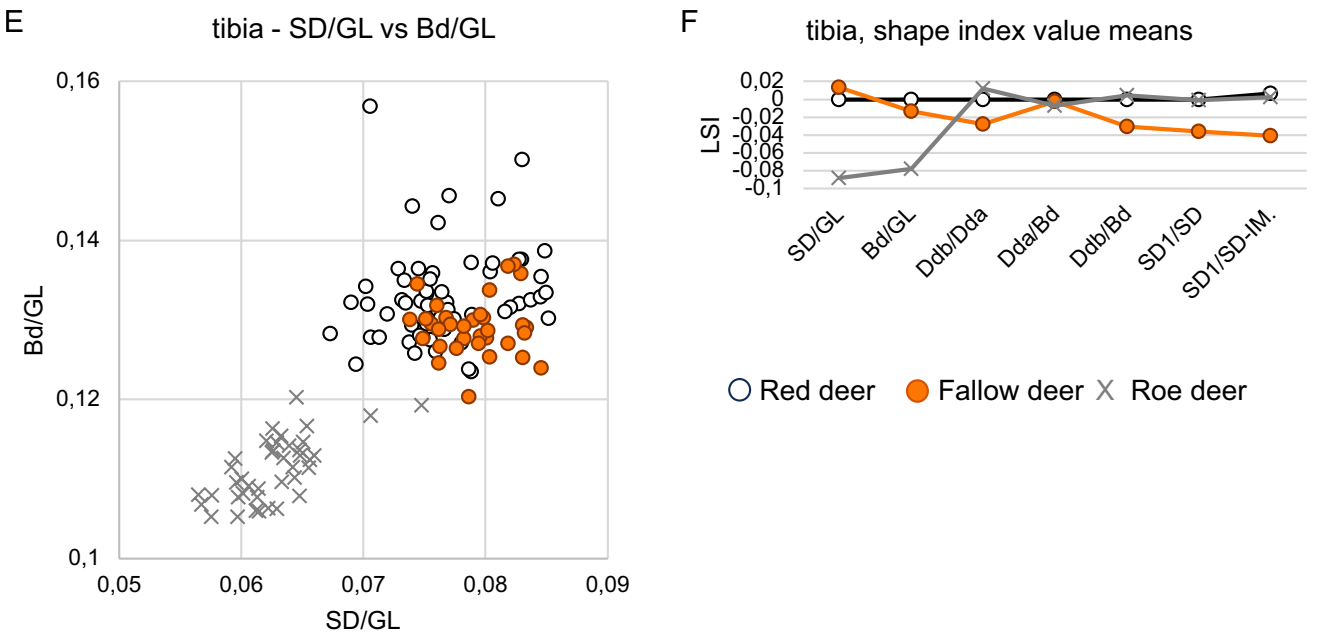

Fig. 8 (continued)

Table 7 *p*-values from Mann–Whitney U tests (MWU) and Student's t-test (St) for the shape indices of the tibia. A graphical representation of the results is available in Online Resource 4: Fig. 5

Mann–Whitney U test and Student's t-test: *p*-values				
Shape index	Fallow-red deer		Fallow-roe deer	
	MWU	St	MWU	St
SD/GL	<0.001	<0.001	<0.001	<0.001
Bd/GL	<0.001	<0.001	<0.001	<0.001
Ddb/Dda	<0.001	<0.001	<0.001	<0.001
Dda/Bd	<0.001	0.002	<0.001	<0.001
Ddb/Bd	<0.001	<0.001	<0.001	<0.001
SD1/SD	<0.001	<0.001	<0.001	<0.001
SD1/SD-IM	<0.001	<0.001	<0.001	<0.001

species, whose shape index average values are higher. The results of statistical tests for the shape index measurements only partly reflect those from data visualization, sometimes producing highly significant differences that do not translate into actual visual separation (Table 8). The results of the PCA, on the other hand, confirm the little efficiency provided by shape index analyses alone in separating astragali from the three cervid species (Online Resource 5: Fig. 7).

Calcaneum

The value ranges of measurements Bd and, to a lesser extent, c highlight some dimensional overlap between fallow deer and red deer, while size overlaps are negligible or absent, in the sample used here, between fallow deer and roe deer (Fig. 10, graphs A, B). Combined with the shape indices Bd/Dd and c/d, however, size differences provide a good separation also between the two larger species, the fallow deer index values plotting higher in graph A and running parallel to red deer's in a bottom-left to top-right direction in graph B, as a consequence of positive allometric relations following different regression lines. The separation potentials of the same shape indices are presented together in graph C. The higher values of the Bd/Dd shape index in fallow deer and roe deer reflect that the dimensions of the calcaneum distal end are proportionally more similar in these species, although the limited extent of such difference and different sizes make this difficult to observe by eye. Similarly, measurement values c and d are proportionally closer in fallow deer and roe deer compared to red deer.

The value ranges of two other shape indices from the proximal end display substantial overlap but with the cluster of red deer values slightly skewed towards the top-right of graph D; this reflects different proportions between the lengths (c, d) and width (B) of the proximal end, roe deer's and especially fallow deer's being 'more slender'. The same shape indices are used to assess the distributions of values from immature specimens (i.e., with unfused distal end); despite the smaller sample sizes, the same observations made for graph D apply to graphs E. The shape index value means (graphs F) are in line with the observations made for graphs A-E, as are the results of statistical tests (Table 9). The results of the PCA provide a better separation of fallow and red deer than that observed on scatter plots, with the exception of immature individuals (Online Resource 5: Figs. 8 and 9).

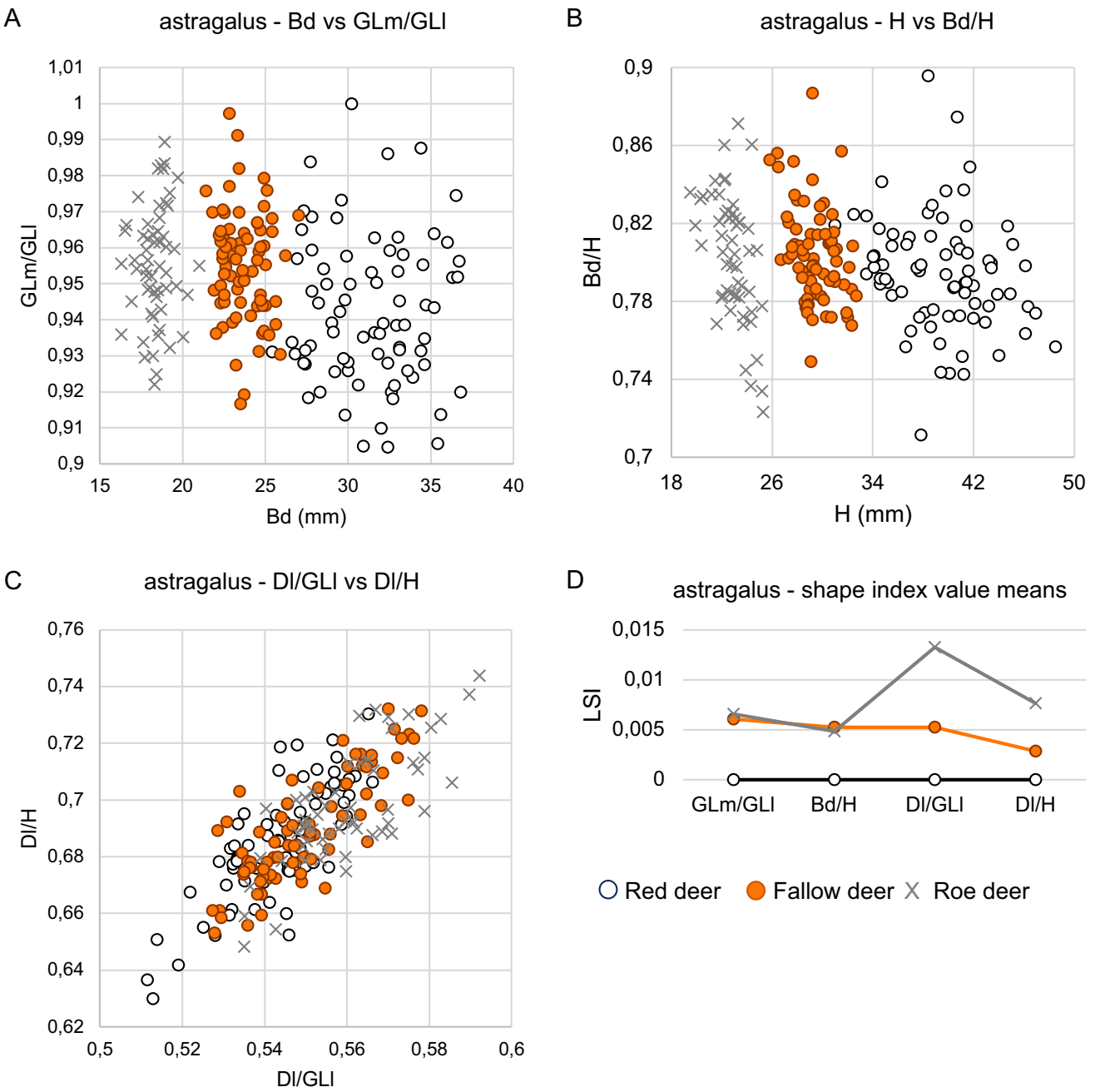

Fig. 9 Size and shape index ranges for the astragalus. For selected combinations of size ranges and shape indices: **A**. Bd vs GLm/GLl; **B**. H vs Bd/H. For two other shape indices: **C**. Dl/GLl vs Dl/H. The means of shape index values from the three species are expressed as LSI values in graph D, using the mean values of red deer indices as the standard (box plots for the shape indices analysed in this study are available in Online Resource 3: Fig. 6)

Metatarsus

The sample used in this paper does not highlight any substantial dimensional overlap of measurement a (width of the medial condyle) values among the three cervid species, with shape index a/2 maximizing the separation of the three clusters (Fig. 11, graph A). Two other shape indices from the medial condyle (a/3 and 3/2, graph B) separate well the values from the three species, creating a clover-shaped distribution. Measurement b (width of the lateral condyle) values present a greater degree of dimensional overlap but the three shape indices work well in enhancing value cluster separations (graphs C, D), with a slightly greater overlap of fallow deer and red deer values in graph D. The consistency of the evidence from both condyles indicates that, in fallow deer, distal widths are proportionally less small than

Table 8 *p*-values from Mann–Whitney U tests (MWU) and Student's t-test (St) for the shape indices of the astragalus. A graphical representation of the results is available in Online Resource 4: Fig. 6

Mann–Whitney U test and Student's t-test: *p*-values				
Shape index	Fallow-red deer		Fallow-roe deer	
	MWU	St	MWU	St
GLm/GLl	<0.001	<0.001	0.734	0.686
Bd/H	0.036	0.032	0.689	0.897
Dl/GLl	0.013	0.002	<0.001	<0.001
Dl/H	0.365	0.164	0.017	0.032

depths compared to red deer's, while in roe deer the dimensional differences between the antero-posterior diameters of the verticillus and of the internal trochlea are proportionally greater than in the two larger species. In addition, similarly to the metacarpus, fallow deer and red deer values from both condyles display positive allometric relations between size and shape index, following different regression lines and thus favouring species separation (graphs A, C).

Graph E plots the proportions between the condylar widths and the total width of the distal articular facet; despite substantial overlaps, the cluster of fallow deer values is slightly skewed to the top-right of the graph, suggesting that, in this species, the two condyles are proportionally closer to each other. In graph F, two other shape indices show that the smallest depth of the diaphysis (SD1) is proportionally smaller in fallow deer. The shaft index (SD1/SD) is also used, along with SD, in graph G: size overlap between fallow deer and red deer is significant but the value clusters from these two species remain well separated through the combination with the shape index; this latter suggests that, as in other elements, fallow deer metatarsus shafts are 'flatter' than in red deer and roe deer. Such characteristic is also detectable in immature specimens, despite some degree of overlap with red deer outlier values (graph H).

In mature specimens, the metatarsus greatest length (GL) values show substantial dimensional overlap between fallow deer and roe deer, and minimal size overlap between the two larger species (graph I). However, all GL shape indices (graphs I, J) highlight the usual greater slenderness of roe deer specimens, while fallow deer and red deer values present positive allometric relations along different regression lines (graph I). In fallow deer, the smaller size of the shaft smallest depth (SD1), proportionally to all other measurements (as well as, to a lesser extent, the proportionally smaller BFd), shows up in graph J, with fallow deer values constrained in the bottom-left part of the red deer value distribution range.

The shape index value means (graph L) broadly support the observations made for graphs A-J. The fallow deer lower SD1/SD index mean value in both mature and immature specimens reflects the flatter shape of the metatarsus shaft of this species, as displayed in graphs F–H. The different dimensional proportions of distal widths and depths in the three cervid species are visible in the fallow deer and roe deer higher LSI mean values of some shape indices from both condyles. The low values of all roe deer robustness indices (SD/GL, SD1/GL, and Bd/GL) reflect the greater slenderness of this species' skeletal elements. The results of statistical tests for the shape index measurements fully support the observations above (Table 10). Also the results of the PCA confirm the excellent degree of separation of red deer, fallow deer, and roe deer specimens (Online Resource 5: Fig. 10).

Discussion

The analysis of size and shape indices highlights a variable degree of success in the separation of red deer, fallow deer, and roe deer values from post-cranial elements.

In mature specimens, size often provides good separation of the three species, from complete separation to mild overlaps. The use of biometric data from populations of northern, central, and southern Europe, including Great Britain and part of the Italian peninsula, where red deer is smaller, allows to display a varying set of size ranges. As suggested in previous sections, however, such dimensional ranges are far from complete. The existence of smaller red deer than the specimens used here is of special concern when the proposed methodology aims to separate this species from the fallow deer, a slightly smaller animal. Iberian, southern Italian, south-eastern European, and north African red deer individuals, on average among the smallest representatives from continental mainlands (Mattioli and Ferretti 2014; Becciolini et al. 2016), are missing in the dataset; similarly, specimens from extant populations inhabiting medium- and small-sized islands, where red deer underwent varying and often complex processes of size decrease (Vigne 1988; Mulville 2010), have not been sampled. In addition, red deer being an especially successful species due to its adaptability, its size fluctuates substantially to fit climatic change, geography, changes in habitat and dietary resources, and hunting pressure, both on long (Lister 1984; Di Stefano et al. 2015) and much shorter chronological scales (Mattioli and Ferretti 2014; Mitchell et al. 1977).

In sum, wider ranges of red deer bone size values than those displayed in this study should be borne in mind, especially regarding the existence (past and present) of smaller red deer. As a consequence, greater degrees of bone dimensional overlaps must be considered in graphs that combine size ranges and shape index values. Nevertheless, the dimensional analyses presented here can at least suggest with which elements and measurements size overlaps are more likely to occur (e.g., the scapula SLC and GLP, the shaft

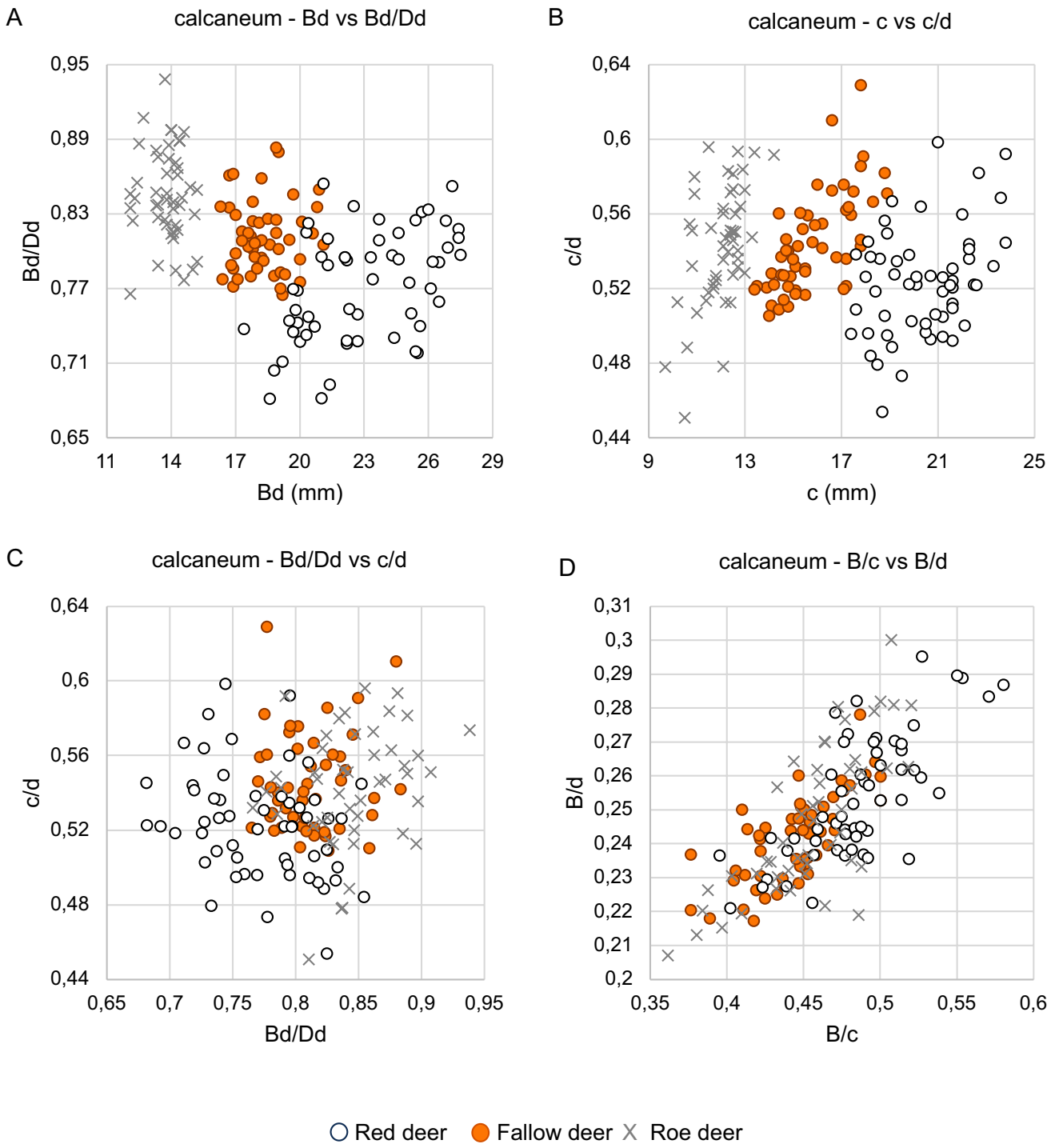

Fig. 10 Size and shape index ranges for the calcaneum. For selected combinations of size ranges and shape indices: **A**. Bd vs Bd/Dd; **B**. c vs c/d. The two shape indices of graphs A, B are plotted together in graph **C**. For two other shape indices: **D**. B/c vs B/d. For immature specimens: **E**. B/c vs B/d. The means of shape index values (**F**) from the three species are expressed as LSI values, using the mean values of red deer indices as the standard (IM.: immature; box plots for the shape indices analysed in this study are available in Online Resource 3: Fig. 7)

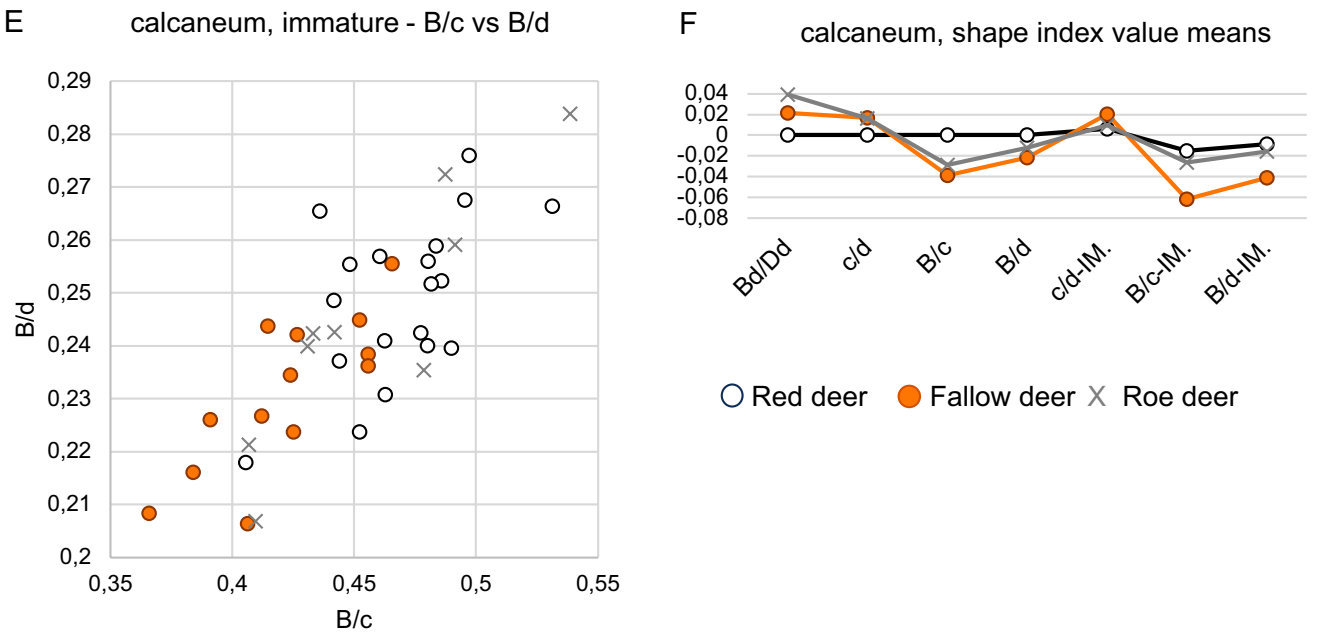

Fig. 10 (continued)

Table 9 *p*-values from Mann–Whitney U tests (MWU) and Student's t-test (St) for the shape indices of the calcaneum. A graphical representation of the results is available in Online Resource 4: Fig. 7

Mann–Whitney U test and Student's t-test: *p*-values				
Shape index	Fallow-red deer		Fallow-roe deer	
	MWU	St	MWU	St
Bd/Dd	<0.001	<0.001	<0.001	<0.001
c/d	<0.001	<0.001	0.704	0.834
B/c	<0.001	<0.001	0.061	0.111
B/d	<0.001	<0.001	0.289	0.137
c/d-IM	0.066	0.078	0.317	0.222
B/c-IM	<0.001	<0.001	0.062	0.052
B/d-IM	0.005	0.003	0.181	0.149

measurements of all elements, in addition to the humerus and calcaneum Bd, the radius Bp, and the metapodials b), and which ones can instead be used more confidently to assist in taxonomic identification (e.g., the astragalus Bd and the metatarsus a).

Shape indices present a varying degree of success in the taxonomic separation of the three species. When separation is provided, by one index or by a combination of two indices, this can either be in terms of isolation of the fallow deer cluster, when its values plot differently from both red deer's and roe deer's (e.g., the scapula ASG/GLP, the combination of humerus indices in graph E, the metapodials shape indices from both condyles, the tibia Ddb/Dda and SD1/SD), or in terms of isolation of one of the other species (e.g., the combination of humerus indices in graph F, the combination of metatarsus indices in graphs E and F). In the latter case, other measurements and shape indices can be plotted, if available, to facilitate or confirm species-level identification. An example is provided by the distal metatarsus, where, in addition to size, two shape indices per condyle allow to separate the three cervids: the width-depth proportions to separate fallow and red deer (a/3 and b/6), and the proportion of two depths for separating fallow and roe deer (3/2 and 6/5) (Fig. 11, graphs B, D).

The different distributions produced by some shape indices reveal subtle morphological differences between species, which had not been previously observed; this may be a reflection of such differences being too slight to be detected by the eye, and/or being more easily missed due to the co-occurrence of size discrepancies. For example, one morphological trait that seems to characterise many fallow deer elements and zones is a distinct proportion between widths and depths, in this species often more in favour of widths: in most elements, the shaft shape index employing the smallest width and depth (SD1/SD) is lower in fallow deer, indicating that its shafts are 'flatter' in comparison to red deer's and roe deer's; similarly, in the metatarsus distal condyles of fallow deer, widths are proportionally less smaller than depths compared to red deer's (Fig. 11, graphs B, D). A more visible morphological trait is the greater depth of the insertion for the lateral ulnar articulation for the radius in red deer (Fig. 6, graph B; probably a reflection of character 6 from Lister (1996: Fig. 2, Part 4 therein)), which prompted the introduction and analysis of measurement V, or, in the same element and zone, the slightly less pronounced lateral bicipital tuberosity of red deer (Fig. 6, graph A). On the other hand, the biometric translation of the diagnostic character from Di Stefano (1995: Fig. 5 therein) on the distal humerus

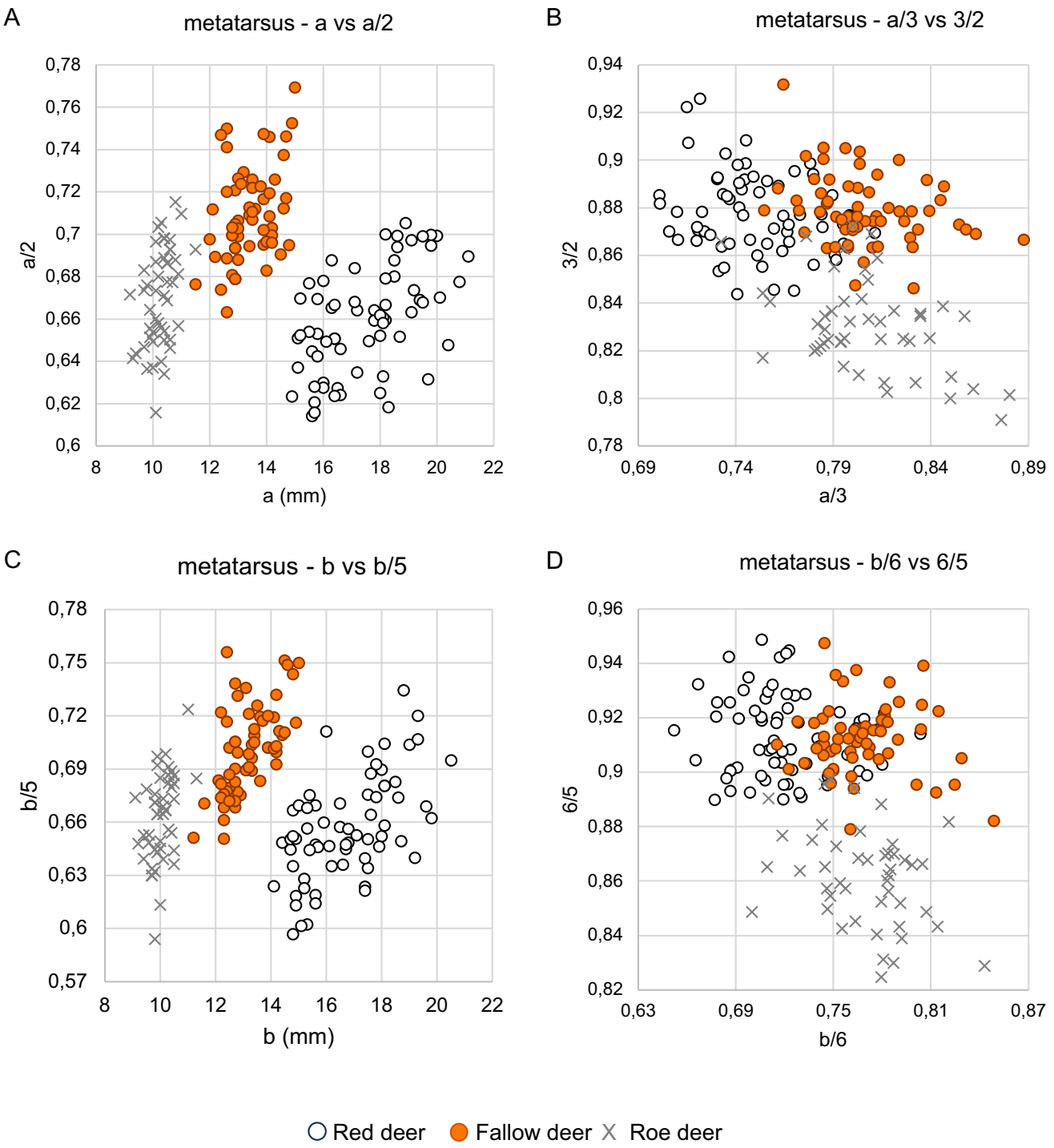

Fig. 11 Size and shape index ranges for the metatarsus. For the distal end: **A**. a vs a/2; **B**. a/3 vs 3/2; **C**. b vs b/5; **D**. b/6 vs 6/5; **E**. a/Bd vs b/Bd. Graph **F** combines distal end and shaft measurements. For the shaft: SD vs SD1/SD for adult (**G**) and immature (**H**) specimens. For overall proportions of complete mature metatarsi: GL vs SD/GL (**I**) and SD1/GL vs Bd/GL (**J**). The means of shape index values (**K**) from the three species are expressed as LSI values, using the mean values of red deer indices as the standard (IM.: immature; box plots for the shape indices analysed in this study are available in Online Resource 3: Fig. 8)

(whereby in fallow deer the trochlea is directed laterally with a more acute angle), achieved by taking multiple height and width measurements, has not been particularly successful, only one index (HX/Bd) possibly reflecting such character (Fig. 5, graph A). Complete bone robusticity indices involving greatest length measurements consistently isolate the roe deer, whose long bones appear far more slender than the other two species'.

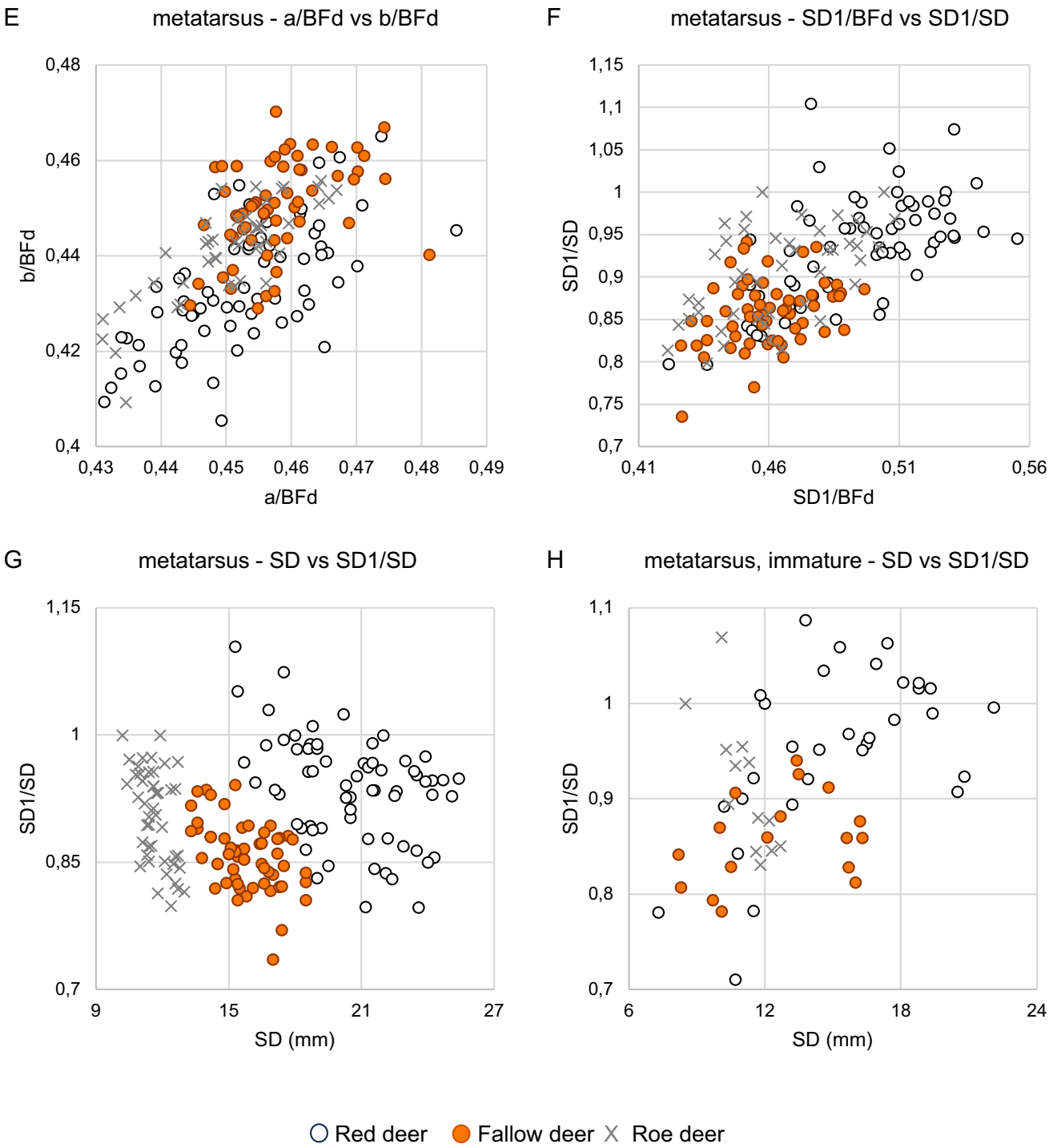

Fig. 11 (continued)

Importantly for the aims of this study, shape index values from immature individuals (long bone shafts, proximal calcaneum) often follow similar distribution patterns to those observed in mature animals; as dimensional separation is more difficult with juvenile specimens, and the degree of ossification alone cannot be used to estimate adult size, these results may prove particularly relevant in the taxonomic identification of remains from younger cervids. In addition, the effectiveness of shaft shape indices (SD1/SD) in mature and immature individuals alike is also very important, as it suggests that it may now be possible to attempt species-level identification of fragmented cervid bones missing either or both ends (where diagnostic morphological criteria are described).

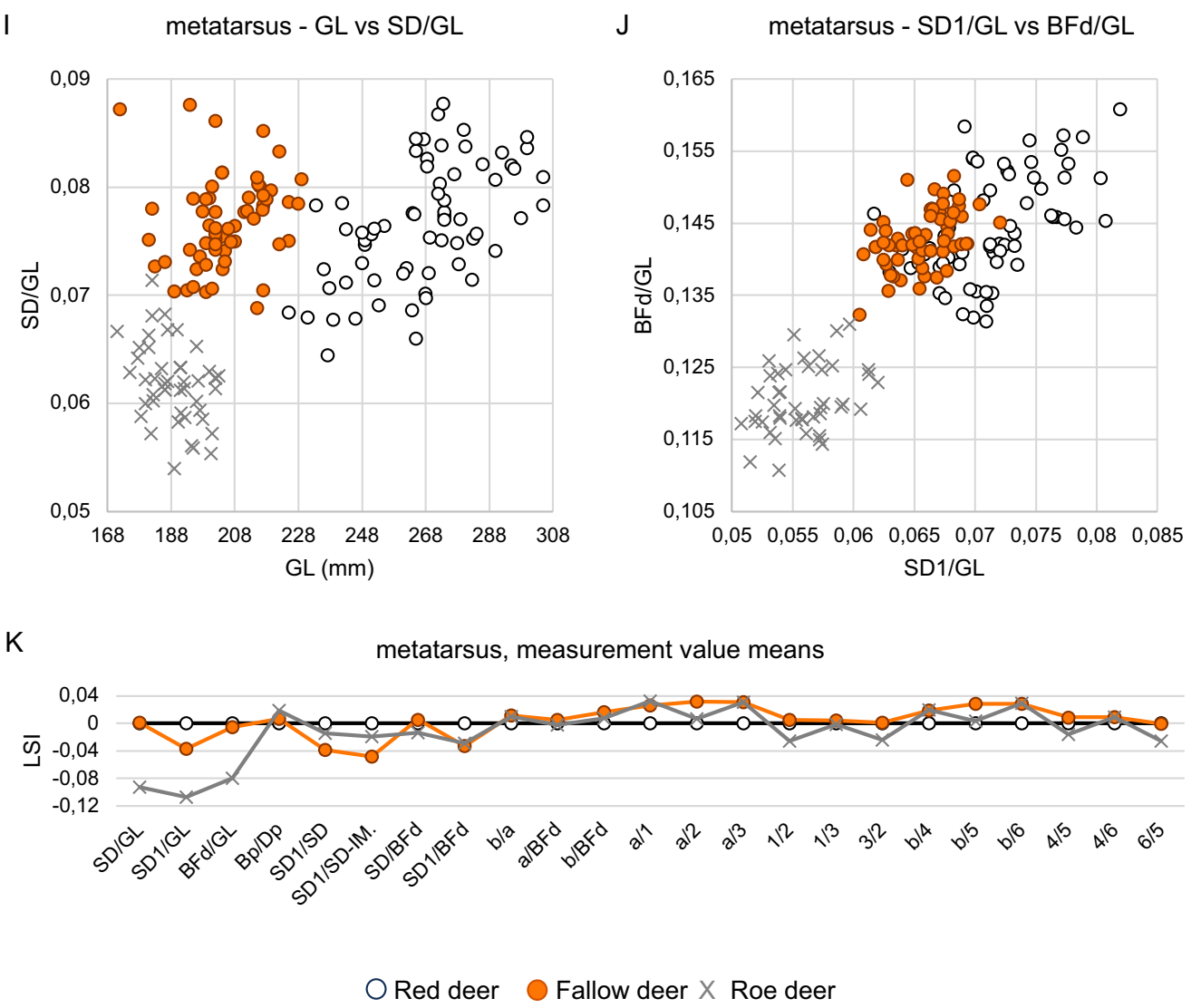

Fig. 11 (continued)

Table 10 *p*-values from Mann–Whitney U tests (MWU) and Student's t-test (St) for the shape indices of the metatarsus. A graphical representation of the results is available in Online Resource 4: Fig. 8

Mann–Whitney U test and Student's t-test: *p*-values									
Shape index	Fallow-red deer		Fallow-roe deer		Shape index	Fallow-red deer		Fallow-roe deer	
	MWU	St	MWU	St		MWU	St	MWU	St
SD/GL	0.915	0.826	<0.001	<0.001	a/2	<0.001	<0.001	<0.001	<0.001
SD1/GL	<0.001	<0.001	<0.001	<0.001	a/3	<0.001	<0.001	0.936	0.886
BFd/GL	0.310	0.107	<0.001	<0.001	1/2	0.007	0.003	<0.001	<0.001
Bp/Dp	0.078	0.178	<0.001	<0.001	1/3	0.018	0.010	0.007	0.005
SD1/SD	<0.001	<0.001	<0.001	<0.001	3/2	0.468	0.641	<0.001	<0.001
SD1/SD-IM	<0.001	<0.001	0.013	0.023	b/4	<0.001	<0.001	0.942	0.720
SD/BFd	0.222	0.154	<0.001	<0.001	b/5	<0.001	<0.001	<0.001	<0.001
SD1/BFd	<0.001	<0.001	0.525	0.609	b/6	<0.001	<0.001	0.438	0.776
b/a	<0.001	<0.001	0.192	0.323	4/5	<0.001	<0.001	<0.001	<0.001
a/BFd	0.007	0.003	<0.001	<0.001	4/6	<0.001	<0.001	0.778	0.988
b/BFd	<0.001	<0.001	<0.001	<0.001	6/5	0.745	0.543	<0.001	<0.001
a/1	<0.001	<0.001	0.035	0.026					

In many instances, graphs combining size and shape index values reveal allometric relations between them. These are important to consider, as they contribute to assess the reliability and potentials of species-level identification. Using the cases reported above, for example, the 'flatness' of the tibia shaft (Fig. 8, graphs C, D), as well as the metatarsus' (Fig. 11, graph G), increases (i.e., SD1/SD values become lower) with size in both fallow deer and red deer, although following different regression curves; this increased flatness is also observed for the distal metatarsus condyles described above, again with red and fallow deer values distributed along distinct curves (Fig. 11, graphs A, C). Similarly, the lateral angle created by the trochlea of the humerus, generally more acute in fallow deer than in red deer (Di Stefano 1995: Fig. 5 therein), becomes increasingly more acute with increased size in both species (Fig. 5, graph A), while the lateral bicipital tuberosity of the proximal radius becomes more pronounced (Fig. 6, graph A). These trends are the result of width measurements presenting a positive allometry (i.e., growing faster than other measurements). Other allometries are visible in the astragalus (Fig. 9, graph B) and the calcaneum (Fig. 10, graph B), in this case also involving the roe deer. The existence of allometries following different regression lines is especially useful in this study, as size and shape index overlaps are partly overcome by the different distributions, along similar ranges, of values from different species. The limited success of the c/d shape index of the calcaneum in taxonomic separation, for example, is overturned when the index is plotted against an absolute measurement, as its values increase with increased size along different regression lines for fallow deer and red deer. On the one hand, these trends highlight the importance of combining size and shape index values to maximise taxonomic separation; on the other, they warn against the acritical use of shape indices, as different shape index value distributions for differently-sized species may also be the result of allometric relations along similar regression curves: this could be the case of the tibia Ddb/Dda index values for the fallow and red deer, although in this case the regression trends remain unclear (Fig. 8, graph A). In this regard, it is also worth noting that, while the little efficiency of the astragalus' shape indices is partly overturned by allometric relations following different regression lines (Fig. 9, graph B), the PCA of shape indices produced three largely overlapping clusters: despite the optimization of taxonomic separation offered by more sophisticated data processing, therefore, the use of the PCA turns out, in this case, to be less efficient than a critical combination of size and shape analyses in scatter plots.

In sum, the results of the biometric analyses highlight that:

- The size ranges for the three species produce different degrees of dimensional overlaps for different elements and measurements, roe deer size values often separating from fallow deer's better than red deer's do;
- The selected shape indices separate the values from the three species with varying degrees of success, alone or in combination with size or other shape indices. Such distinct distributions are a reflection of both previously undetected and published morphological differences;
- Some shape indices remain effective when applied to the taxonomic separation of immature individuals, for which size overlaps are substantial and prevent identification;
- Shaft shape indices are often effective, extending species-level identification attempts to fragmented materials with no published diagnostic morphological traits;
- The value distribution of many shape indices, plotted against size, reveal the existence of allometric relations between them. In many instances, such allometries rely on different regression lines for different species, amplifying the taxonomic separation potentials of combined shape and size analyses.
- The results of PCA analysis of shape indices often reflect and sometimes reinforce the taxonomic separations provided by the comparisons of size and shape index value ranges presented in scatter plots, linear graphs, and box plots; however, it should be used alongside these latter analyses, to ensure a critical use of both size and shape data.

Conclusions

The biometric analyses presented in this paper rely on data from nine modern reference collections and different European regions. They describe dimensional and morphological criteria that can be used to assist species-level identification of archaeological cervid bones. This is especially important for the separation of fallow deer remains; despite its known historical and ecological significance, indeed, this relatively rarer species has often been overlooked and sometimes its bones misidentified in European zooarchaeological research, leading to limited visibility in the archaeological record. Such underestimation biases our understanding of past human-cervid-environment interactions, calling for more accurate and objective approaches such as the one offered by this biometric method.

The obtained results show that size remains important evidence to use with caution, while the clustering of shape index values separately for the three species, despite the disparate origins of the modern skeletons, indicates that the method can be applied to materials from different regions and time periods. In addition, the many allometric relations

between size and shape index values seem to support the existence of broadly similar morphometric characters; the often-different regression lines followed by such relations in each species prove useful in species-level separation.

Only two published morphological diagnostic criteria (Di Stefano 1995: Fig. 5 therein; Lister 1996: Fig. 2, Part 4, character 6 therein) were translated biometrically; all other shape indices reflect more subtle differences and can be considered 'new' evidence. This characterises the method proposed here as an independent, complementary tool to use *in addition* to others (use of appropriate reference collections, assessment of morphological criteria).

Equally important is the fact that the method is grounded in what are now frequently referred to—often with a somewhat dismissive connotation—as 'traditional analyses', as it consists of straightforward biometry. In a research landscape increasingly spellbound by techniques such as ZooMS, ancient DNA, and isotopic analyses, this study offers a timely and valuable re-evaluation of foundational methods. While scientifically advanced techniques undoubtedly expand the analytical potentials of faunal research, they often require substantial financial investment, specialised equipment and staff, and access to dedicated laboratory infrastructures—resources that are not always readily available to researchers. In addition, the (justified) sense of novelty conveyed when these techniques start being applied to certain materials, animal species, regions or periods, as well as the greater consideration implied by higher resource investments, may often lead to neglecting a proper integration of results with other lines of zooarchaeological evidence and within the broader archaeological and historical context. It has now become important to remind and value the primary role of methodologically sound and cost-effective 'traditional analyses', firmly grounded in archaeological reasoning and accessible to all.

Supplementary Information The online version contains supplementary material available at https://doi.org/10.1007/s12520-025-02380-7.

Acknowledgements The method presented in this paper is the first output of the Cervified Project, conducted by the authors to investigate the potential of biometric approaches for species-level identification of archaeological European cervid remains, as well as for the study of past and present cervid bone morphometry. The authors are grateful to the institutions they visited for data collection: the former Department of Archaeology of the University of Sheffield (UK), Historic England (Fort Cumberland, UK), the Department of Natural History of the University-Museum of Bergen (Norway), the Natural History Museum in Vienna (Austria), the Hungarian Natural History Museum (Budapest, Hungary), the Malcolm H. Wiener Laboratory for Archaeological Science of the American School of Classical Studies at Athens (Greece), the Department of Physical Sciences, Earth and Environment of the University of Siena (Italy), and the Natural History Museum of Venice (Italy). The data collection trip to Historic England also allowed to measure the modern deer from the private reference collection of Sheila Hamilton Dyer (Southampton, UK), who kindly made her specimens available. The authors are thankful to the many colleagues and friends who provided useful suggestions and comments: Umberto Albarella, Polydora Baker, Simon Davis, Kostantina Saliaris, and László Bartosiewicz. We would also like to thank (in alphabetical order) Umberto Albarella, Stephanie Baron, Marina Chorro-Giner, Steve Hollings, Phoebe Liu, Maeve Moorcroft, Mya Pearce-Ahdoud, Matt Rayner, and Lenny Salvagno for their contribution to the estimation of the inter-observer error, as well as three anonymous peer reviewers for their insightful comments. A heartfelt thank you to Silvia Valenzuela Lamas for her support in data processing using R, and to Bjorn Reidar Olsson for providing alive deer pictures. This research was also supported by the Beatriu de Pinós fellowship (Generalitat de Catalunya, Agència de Gestió d'Ajuts Universitaris i de Recerca, co-funded by the EU Horizon 2020 MSCA programme) awarded to Veronica Aniceti. Finally, a special thought goes to the Zooarchaeology Laboratory at the University of Sheffield, whose reference collection we came to know very well - learning from it, improving it, and exploring its potential for collaborative teaching and research. We are grateful to have had the opportunity to visit it and use it before the ill-conceived decision was made to relocate it to a wholly unsuitable venue for an internationally renowned reference collection and to impose prohibitively high access fees, rendering it inaccessible to most. This stands in stark contrast to the inclusive ethos we experienced and grew up with in Sheffield - the same ethos this paper seeks to uphold and promote. This move is part of the broader undermining of the Department of Archaeology by the University, culminating in its recent closure. To our friends and colleagues in Sheffield, we offer our heartfelt support and solidarity.

Author contribution VA, MR: Conceptualisation, Methodology, Formal analysis, Data Curation, Data processing, Writing—Original Draft, Review and Editing, Visualisation, Funding acquisition. FG: Data curation, Data processing, Visualisation.

Funding Open Access funding provided thanks to the CRUE-CSIC agreement with Springer Nature. A series of grants contributed to the collection of biometric data from modern reference specimens: the Postgraduate Researcher Experience Programme grant (University of Sheffield, UK, https://www.sheffield.ac.uk/) (MR), the Strategic P rogramme for International Research and Education (SPIRE) visiting fellowship grant (University- Museum of Bergen, Norway, https://www.uib.no/en/universitymuseum) (MR), and two Synthesys+ Transnational Access - Taxonomic Access Facility grants (European Commission, https://www.synthesys.info/access/transnationalaccess.html) (VA). Open access to this publication was supported by a Beatriu de Pinós fellowship (Generalitat de Catalunya, Agència de Gestió d'Ajuts Universitaris i de Recerca, https://agaur.gencat.cat/en/Beatriu-de-Pinos, cofunded by the EU Horizon 2020 MSCA Programme, grant n. 2022 BP 00207) awarded to VA. The funders had no role in study design, data collection and analysis, decision to publish, or preparation of the manuscript.

Data availability The CERVIFIED Database is available in Mendeley Data: https://data.mendeley.com/datasets/vn43dpvbzr/1 https://doi.org/10.17632/vn43dpvbzr.1

Declarations

Competing interests The authors declare no competing interests.

References

Albarella U, Aniceti V (2024) "Unmaking" the deer in medieval Europe: historical and archaeological evidence. Eur J Archaeol 27(3):1–19. https://doi.org/10.1017/eaa.2024.11

Albarella U, Davis S (1996) Mammals and birds from Launceston Castle, Cornwall: decline in status and the rise of agriculture. Circaea 12(1):1–156

Albarella U (2002) 'Size matters': how and why biometry is still important in zooarchaeology. In K. Dobney, & T. P. O'Connor (Eds.), *Bones and the man. Studies in honour of Don Brothwell* (pp. 51–62). Oxbow

Almeida NJ, Guinot C, Ribeiro I, Barreira J, Basílio AC (2024) Human-deer relations during late prehistory: the zooarchaeological data from central and southern Portugal in perspective. Animals 14(10):1424. https://doi.org/10.3390/ani14101424

Aniceti V, Albarella U, Sebastiani A (2021) The faunal assemblage from the manufacturing district at Spolverino: from the Roman Imperial period to Late Antiquity. Archaeofauna 30:167–183. https://doi.org/10.15366/archaeofauna2021.30.009

Apollonio M, Chirichella R (2023) Deer and climate change: impacts and perspectives. Anim Prod Sci 63(16):1573–1582. https://doi.org/10.1071/AN22296

Baker KH, Gray HWI, Lister AM, Spassov N, Welch AJ, Trantalidou K, Rose H, Schroeder H, Hoelzel AR (2024a) Ancient and modern DNA track temporal and spatial population dynamics in the European fallow deer since the Eemian interglacial. Sci Rep 14:3015. https://doi.org/10.1038/s41598-023-48112-6

Baker KH, Miller H, Doherty S, Gray HWI, Daujat J, Çakırlar C, Love S, Zant JM, Cooper A, Irving-Pease EK, Burger J, Rose H, Thomas R, Ross-Piper J, Bradfield J, Linderholm A, Boessenkool S, Biebach I, Schroeder H, Hoelzel AR (2024b) The 10,000-year biocultural history of fallow deer and its implications for conservation policy. Proc Natl Acad Sci 121(8):e2310051121. https://doi.org/10.1073/pnas.2310051121

Becciolini V, Bozzi R, Viliani M, Biffani S, Ponzetta MP (2016) Body measurements from selective hunting: biometric features of red deer (*Cervuselaphus*) from Northern Apennine, Italy. Italian J Animal Sci 15(3):461–472. https://doi.org/10.1080/1828051X.2016.1186505

Beglane F, Baker KH, Carden R, Hoelzel R, Lamb A, Fhionnghaile R, Vernesi C, Mattingly A, Gooley R, Chechushkov I, Irving-Pease E (2018) Ireland's fallow deer: their historical, archaeological and biomolecular records. Proc R Ir Acad Archaeol Cult Hist Lit 118C:141–165. https://doi.org/10.3318/priac.2018.118.01

Boessneck J, Muller HH, Teichert M (1964) Osteologische unterscheidungsmerkmale zwischen Schaf (Ovis aries Linne) und Ziege (Capra hircus Linne). Kuhn Arch 78:1–129

Bowen F, Carden RF, Daujat J, Grouard S, Miller H, Perdikaris S, Sykes N (2016) Dama dentition: a new tooth eruption and wear method for assessing the age of fallow deer (*Dama dama*). Int J Osteoarchaeol 26:1089–1098. https://doi.org/10.1002/oa.2523

Buckley M, Whitcher Kansa S (2011) Collagen fingerprinting of archaeological bone and teeth remains from Domuztepe, South Eastern Turkey. Archaeol Anthropol Sci 3(3):271–280. https://doi.org/10.1007/s12520-011-0066-z

Carden RF, McDevitt AD, Zachos FE, Woodman PC, O'Toole P, Rose H, Monaghan NT, Campana MG, Bradley DG, Edwards CJ (2012) Phylogenetic, ancient DNA, fossil and morphometric analyses reveal ancient and modern introductions of a large mammal: The complex case of red deer (Cervus elaphus) in Ireland. Quatern Sci Rev 42:74–84. https://doi.org/10.1016/j.quascirev.2012.02.012

Chapman D, Chapman N (1975) Fallow deer: Their history, distribution and biology. Terence Dalton Ltd

Davis SJM (1996) Measurements of a group of adult female Shetland sheep skeletons from a single flock: a baseline for zooarchaeologists. J Archaeol Sci 23(4):593–612. https://doi.org/10.1006/jasc.1996.0056

Davis SJM, MacKinnon M (2009) Did the Romans bring fallow deer to Portugal? Environ Archaeol 14:15–26. https://doi.org/10.1179/174963109X400646

Di Stefano G (1995) Identification of fallow deer remains on the basis of its skeletal features: taxonomical considerations. Boll Soc Paleontol Ital 34(3):323–331

Di Stefano G, Pandolfi L, Petronio C, Salari L (2015) The morphometry and the occurrence of Cervus elaphus (Mammalia, Cervidae) from the Late Pleistocene of the Italian peninsula. Rivista Italiana di Paleontologia e Stratigrafia 121(1):103–120. https://doi.org/10.13130/2039-4942/6402

Driesch A von den (1976) A guide to the measurement of animal bones from archaeological sites. Peabody Museum Bulletin 1. Peabody Museum of Archaeology and Ethnology

Fernández H (2001) *Ostéologie comparée des petits ruminants euroasiatiques sauvages et domestiques (genres Rupicapra, Ovis, Capra et Capreolus): Diagnose différentielle du squelette appendiculaire* [Doctoral dissertation, University of Geneva, Switzerland]. https://archive-ouverte.unige.ch/unige:77284

Grant A (1988) Food, status and religion in England in the Middle Ages: An archaeozoological perspective. Anthropozoologica 2:139–146

Heurich M, Zeis K, Küchenhoff H, Müller J, Belotti E, Bufka L, Woelfing B (2016) Selective predation of a stalking predator on ungulate prey. PLoS One 11(8):e0158449. https://doi.org/10.1371/journal.pone.0158449

Holmes M (2014) Making a fast buck in the Middle Ages: Evidence for poaching from medieval Wakefield. In K. Baker, R. Carden, & R. Madgwick (Eds.), *Deer and people* (pp. 200–207). Oxbow Books. https://doi.org/10.2307/j.ctv13gvgms.20

Karastoyanova N, Gorczyk J, Spassov N (2020) The natural history of the fallow deer, *Dama dama* (Linnaeus, 1758) in Bulgaria in prehistory and new evidence for the existence of an autochthonous Holocene population in the Balkans. Int J Osteoarchaeol 30(5):616–628. https://doi.org/10.1002/oa.2886

Kjellander P, Gaillard J-M, Hewison M, Liberg O (2004) Predation risk and longevity influence variation in fitness of female roe deer (*Capreolus capreolus* L.). Proc R Soc Lond B Biol Sci 271(Suppl 5):S338–S340. https://doi.org/10.1098/rsbl.2004.0177

Koo TK, Li MY (2016) A guideline of selecting and reporting intraclass correlation coefficients for reliability research. J Chiropr Med 15:155–163. https://doi.org/10.1016/j.jcm.2016.02.012

Léon P, Garcia MA (1981) *Atlas ostéologique pour servir à l'identification des mammifères du quaternaire*. Centre National de la Recherche Scientifique

Lister AM (1984) Evolutionary and ecological origins of British deer. Proc R Soc Edinb Sect B Biol Sci 82(4):205–229. https://doi.org/10.1017/S0269727000003754

Lister AM (1989) Rapid dwarfing of red deer on Jersey in the last interglacial. Nature 342:539–542. https://doi.org/10.1038/342539a0

Lister AM (1996) The morphological distinction between bones and teeth of fallow deer (Dama dama) and red deer (Cervus elaphus).

Int J Osteoarchaeol 6(2):119–143. https://doi.org/10.1002/(SICI)1099-1212(199603)6:2%3c119::AID-OA265%3e3.0.CO;2-8

Marín J, Saladié P, Azorit C, Rodríguez-Hidalgo A (2024) Identification of age at death in red deer (*Cervuselaphus*) through the upper dentition: eruption pattern, wear stage and crown heights. J Archaeol Sci 163:105934. https://doi.org/10.1016/j.jas.2023.105934

Masseti M, Vernesi C (2014) Historic zoology of the European fallow deer, Dama dama dama: Evidence from biogeography, archaeology and genetics. In K. Baker, R. Carden, & R. Madgwick (Eds.), *Deer and people* (pp. 13–22). Oxbow Books. https://doi.org/10.2307/j.ctv13gvgms.6

Mattioli S, Ferretti F (2014) Morphometric characterization of Mesola red deer *Cervus elaphus italicus* (Mammalia: Cervidae). Ital J Zool 81(1):144–154. https://doi.org/10.1080/11250003.2014.895432

McDevitt AD, Zachos FE (2014) Genetic analyses of natural and anthropogenic movements in deer. In K. Baker, R. Carden, & R. Madgwick (Eds.), *Deer and people* (pp. 2–12). Oxbow Books. https://doi.org/10.2307/j.ctv13gvgms.5

McElligott AG, Gammell MP, Harty HC, Paini DR, Murphy DT, Walsh JT, Hayden TJ (2001) Sexual size dimorphism in fallow deer (*Dama dama*): do larger, heavier males gain greater mating success? Behav Ecol Sociobiol 49:266–272. https://doi.org/10.1007/s002650000293

Meadow RH (1999) The use of size index scaling techniques for research on archaeozoological collections from the Middle East. In C. Becker, H. Manhart, J. Peters, & J. Schibler (Eds.), *Historia animalium ex ossibus. Beiträge zur Paläoanatomie, Archäologie, Ägyptologie, Ethnologie und Geschichte der Tiermedizin. Festschrift für Angela von den Driesch* (pp. 285–300). Verlag Marie Leidorf GmbH

Miller H, Sykes N (2016) Zootherapy in archaeology: the case of the fallow deer (*Dama dama dama*). J Ethnobiol 36(2):257–276. https://doi.org/10.2993/0278-0771-36.2.257

Milošević-Zlatanović S, Tomašević Kolarov N, Vukov T, Stamenković S (2016) Correlation patterns in roe deer cranium: sexual dimorphism across different habitats. J Zool 300(4):291–304. https://doi.org/10.1111/jzo.12383

Mitchell B, Staines BW, Welch D (1977) Ecology of red deer: A research review relevant to their management in Scotland. Institute of Terrestrial Ecology

Mulville J (2010) Red deer on Scottish islands. In T. O'Connor & N. Sykes (Eds.), *Extinctions and invasions: A social history of British fauna* (pp. 43–50). Windgather Press. https://doi.org/10.2307/j.ctv13gvg6k.12

Payne S (1969) A metrical distinction between sheep and goat metacarpals. In: Ucko PJ, Dimbleby GW (eds) The domestication and exploitation of plants and animals. Duckworth, pp 295–305

Payne S, Bull G (1988) Components of variation in measurements of pig bones and teeth, and use of measurements to distinguish wild from domestic remains. Archaeozoologia 2:27–66

Poland JG (2018) A methodological approach to the identification of duck and goose remains from archaeological sites [Doctoral dissertation, University of Sheffield, UK] https://etheses.whiterose.ac.uk/id/eprint/21445/

Post E, Langvatn R, Forchhammer MC, Stenseth NC (1999) Environmental variation shapes sexual dimorphism in red deer. Proc Natl Acad Sci U S A 96(8):4467–4471. https://doi.org/10.1073/pnas.96.8.4467

Prat F (1970–1975) *Quelques mammifères pléistocènes. Odontologie, ostéologie*. Université Bordeaux 1, Institut du Quaternaire

R Core Team (2025) R: A language and environment for statistical computing. R Foundation for Statistical Computing, Vienna, Austria. https://www.R-project.org/

Salvagno L, Albarella U (2017) A morphometric system to distinguish sheep and goat postcranial bones. PLoS One 12(6):e0178543. https://doi.org/10.1371/journal.pone.0178543

Schmidt KT (2014) Supplemental feeding and our attitude towards red deer and natural mortality. In K. Baker, R. Carden, & R. Madgwick (Eds.), *Deer and people* (pp. 270–279). Oxbow Books. https://doi.org/10.2307/j.ctv13gvgms.27

Serrano E, Angibault J-M, Cargnelutti B, Hewison AJM (2007) The effect of animal density on metacarpus development in captive fallow deer. Small Ruminant Res 72(1):61–65. https://doi.org/10.1016/j.smallrumres.2006.07.007

Skog A, Zachos FE, Rueness EK, Feulner PGD, Mysterud A, Langvatn R, Lorenzini R, Hmwe SS, Lehoczky I, Hartl GB, Stenseth NC, Jakobsen KS (2009) Phylogeography of red deer (*Cervus elaphus*) in Europe. J Biogeogr 36(1):66–77. https://doi.org/10.1111/j.1365-2699.2008.01986.x

Soderberg J (2004) Wild cattle: red deer in the religious texts, iconography, and archaeology of early medieval Ireland. Int J Hist Archaeol 8:167–183. https://doi.org/10.1007/s10761-004-1135-0

Sykes N, Carden R, Harris K (2013) Changes in the size and shape of fallow deer — evidence for the movement and management of a species. Int J Osteoarchaeol 23(1):55–68. https://doi.org/10.1002/oa.1239

Sykes N, Ayton G, Bowen F, Baker K, Baker P, Carden R, Hammon C, Ingrem C, Madgwick R, Miller H, Poole K, Rowley-Conwy P, Worley F, Evans J (2016) Wild to domestic and back again: The dynamics of fallow deer management in medieval England (c. 11th-16th century AD). Sci Technol Archaeological Res 2(1):113–126. https://doi.org/10.1080/20548923.2016.1208027

Toïgo C, Gaillard J-M, Laere G, Hewison A, Morellet N (2006) How does environmental variation influence body mass, body size, and body condition? Roe deer as a case study. Ecography 29:301–308. https://doi.org/10.1111/j.2006.0906-7590.04394.x

Tomek T, Bocheński ZM (2009) A key for the identification of domestic bird bones in Europe: Galliformes and Columbiformes. Institute of Systematics and Evolution of Animals, Polish Academy of Sciences

Vigne J-D (1988) *Les mammifères post-glaciaires de Corse: Étude archéozoologique*. Gallia Préhistoire Suppl. 26. Éditions du Centre National de la Recherche Scientifique

Wickham H, Chang W, Henry L, Pedersen TL, Takahashi K, Wilke C, Woo K, Yutani H, Dunnington D, van den Brand T (2025) ggplot2: Create elegant data visualizations using the grammar of graphics. R package version 3.5.2. http://CRAN.R-project.org/package=ggplot2